Supporting Information

Investigation the influence factors on the selectivity and response time of the glyoxal-selective probe

Yuanyuan Wu[a,b] Chang Liu,[*a,b] Huirong Yao,[*a,b] Song He,[a,b] Liancheng Zhao[c] and Xianshun Zeng[*a,b]

[a] *Tianjin Key Laboratory for Photoelectric Materials and Devices, School of Materials Science & Engineering, Tianjin University of Technology, Tianjin 300384, China. Email: xshzeng@tjut.edu.cn.*

[b] *Key Laboratory of Display Materials and Photoelectric Devices, Ministry of Education, School of Materials Science & Engineering, Tianjin University of Technology, Tianjin, 300384, China.*

[c] *School of Materials Science and Engineering, Institute of Information Functional Materials& Devices, Harbin Institute of Technology, Harbin, 150001, China*

1. General information

During the experimental process, all chemicals and reagents were commercially sourced and used directly without further purification, unless otherwise indicated. The water used in the spectral analysis was ultrapure water without fluorescent impurities.

^{1}H NMR and ^{13}C NMR spectra were recorded on a Bruker AVANCE III HD 400MHz spectrometer using tetramethylsilane (TMS) as internal standard. High resolution mass spectra (HRMS) were obtained on an Agilent 6510 Q-TOF LC/MS instrument (Agilent Technologies, Palo Alto, CA) equipped with an electrospray ionization (ESI) source. Melting points were recorded on a RY-2 apparatus (Tianjin, China). UV-vis spectra were recorded by a Shimadzu UV-2550 UV/Vis spectrophotometer with 1 cm standard quartz cell. Fluorescence emission spectra were obtained by a Hitachi F-4600 spectro fluorophotometer with a 1 cm standard quartz cell. The pH measurements were carried out on a Mettler Toledo Seven Excellence pH meter (Mettler Toledo MP 220, Shanghai, China). The absorbance for MTT analysis was recorded on a microplate reader (PL-9602, Beijing, China). Cells imaging was performed using Olympus FV1000-IX81 inverted confocal microscope. All images were analyzed with Olympus FV1000-ASW.

2. Determination of octanol-water partition coefficient of the probe 3

The lipid solubility of the probe **3** was characterised by n-octanol-water partition coefficient (KOW)[S1], which was measured as follows: 50 mL n-octyl alcohol was mixed with 50 mL ultra-pure water, stirred at a constant temperature for 24 h, and stored separately after standing for layering. 10 mL of n-octanol saturated with water

of 5 μM was configured separately and its absorbance at 469 nm was recorded, similarly 10 mL of water saturated with n-octanol of 5 μM was configured and its absorbance at 479 nm was recorded. The molar extinction coefficients (ε) in n-octanol and aqueous phases were obtained by Lambert-Beer law. Then 5 mL water phase containing **3** was added to 5 mL n-octanol phases containing **3**, which was shaken for 1 h and subsequently allowed to stand until completely layered. The upper n-octanol was taken and its absorbance at 469 nm was determined and the concentration of probe was calculated as C_1, the same method was used to obtain the concentration of the probe in the aqueous phase C_2. The KOW value was expressed in terms as Log P, according to the equation:

$$Log\ P = Log\ \frac{C_1}{C_2}$$

3. Determination of the fluorescence quantum yield

Fluorescence quantum yield (Φ) was determined using rhodamine B (Φ_S=0.71, in ethanol) as the fluorescence standard[S2]. The quantum yield was calculated using the following equation:

$$\Phi = \Phi_S \times \frac{A_S \times F \times \lambda_{exS} \times \eta}{A \times F_S \times \lambda_{ex} \times \eta_S}$$

Where Φ and Φ_S represented the fluorescence quantum yields of the target substance and rhodamine B, respectively. F and F_S indicated the peak fluorescence emission of the target substance and rhodamine B, respectively. A and A_S denoted the maximum absorbance values of the target substance and rhodamine B, respectively. η and η_S were the refractive index of the solvent of the target substance and rhodamine B.

4. Determination of detection limit (LOD)

The standard deviation of the blank was determined by 11 measurements of the fluorescence emission spectra of **3** (5 μM). The linear relationship between the concentration of GO and the fluorescence intensity at 612 nm was determined by fitting a concentration-dependent fluorescence curve. The limit of detection (LOD) was calculated using the following equation [9b]:

$$\mathrm{LOD} = 3\sigma / k$$

Where σ was the standard deviation of the blank sample, k was the slope of the linear regression formula.

5. Cells culture and cell viability assay

HeLa cells were cultured in DMEM medium supplemented with 10% fetal bovine serum (FBS) and 1% antibiotics under an atmosphere of 5% CO_2 at 37 ℃. MTT assay was performed to evaluate the cytotoxicity of **3** in living cells. 10000 cells were seeded onto 96 well tissue culture plates under sterile conditions and grown for 12 h. Then, HeLa cells were incubated with different concentrations (0 μM, 1 μM, 2μM, 5 μM, 10 μM and 20 μM) of the probe in DMEM medium supplemented and allowed to cultivated for 24 h. The assay of each concentration needed to be repeat 4 times. After medium removal, cells in each well were treated with 10 μL MTT solution (5 mg/mL) and incubated for another 4 h. Cells were treated with 100 μL DMSO at 37 ℃ for 2 h before measurement. The OD_{630} data for each well were recorded on PL-9602. Cell survival rate was calculated using the formula [S3]:

$$\text{Cell viability} = (\mathrm{OD_{Test}} - \mathrm{OD_{Background}}) / (\mathrm{OD_{Blank}} - \mathrm{OD_{Background}})$$

6. Preparation of real samples

All samples were obtained from a supermarket, and the sample solutions were filtered to remove solid particles prior to conducting the spike recovery experiment.

Preparation of honey: 1 g of honey sample was dissolved in 10 mL PBS buffer for 2 h; Preparation of pastries: 1g sample was soaked in a brown sample bottle with 10 mL of PBS buffer for 2 h; Preparation of paper: A precisely measured 1 g sample of shredded paper, cut into 1×1 cm^2 under conditions that avoided direct skin contact, was subsequently immersed overnight in 10 mL PBS buffer overnight; Preparation of cosmetics: 1g sample was dissolved in 10 mL PBS buffer for 2 h.

7. Abbreviations

$CHCl_3$- Chloroform, DCM- Dichloromethane, DMF- Dimethylformamide, DMSO- Dimethylsulfoxide, EtOAc- Ethylacetate, EtOH- Ethanol, MeCN- Acetonitrile, MeOH- Methanol, THF- Tetrahydrofuran, GO- Glyoxal, MGO- Methylglyoxal, FA- Formaldehyde, Mito- Mitochondria, Lyso- lysosome, LD- Lipid droplet, ER- Endoplasmic reticulum, Golgi- Golgi apparatus.

8. Experiment data

Table S1 Summary of fluorescence probes for glyoxal

Name	Structure	Selectivity	λ_{em} (nm)	Time (min)	LOD_{GO} (μM)	Organlle-Targeting	Reference
L	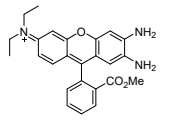	FA, GO, MGO	642	--	--	--	[8a]
NAP-DCP-1	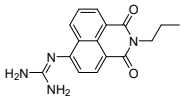	GO, MGO	564	30	0.58	ER-Targeting	[8b]
NAP-DCP-3	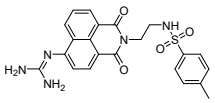	GO, MGO	564	30	0.16	ER-targeting	[8b]
DAN		FA, GO, MGO	411	8	3.97	--	[8c]
DAS		FA, GO, MGO	465	＞60	0.70	--	[8d]
ANC-DCP-1	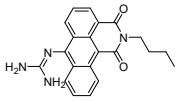	GO, MGO	615	＞120	12.10	--	[8e]
SWJT-18	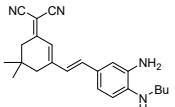	GO	646	15	0.34	--	[8f]
GL1	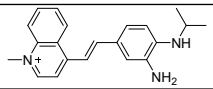	GO	640	＞60	0.021	Mito-targeting	[8g]
Photo-ER-GOS	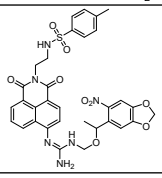	MGO GO	564	120	0.35	ER-targeting	[8h]
1	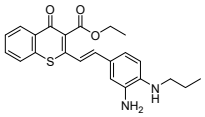	**GO**	**615**	**120**	**0.99**	**Mito-targeting**	**This work**
2	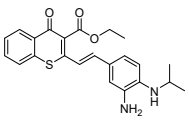	**GO**	**615**	**90**	**0.23**	**Mito-targeting**	
3	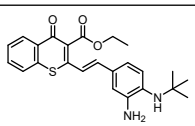	**GO**	**612**	**60**	**0.40**	**Mito-targeting**	
4	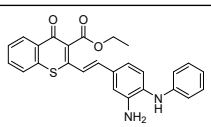	**GO**	**610**	**60**	**4.13**	**Mito-targeting**	

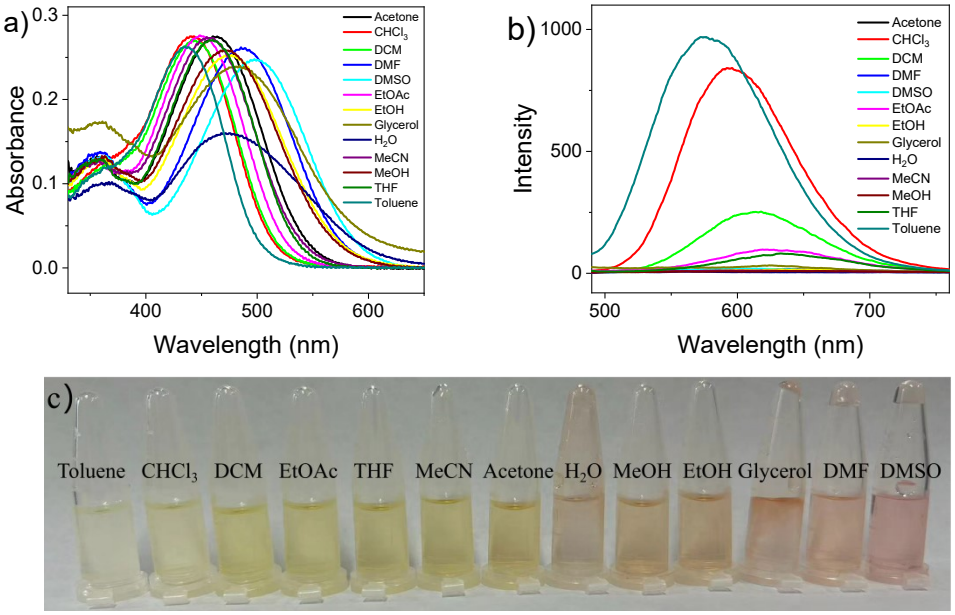

Fig. S1. a) UV/vis absorption (10 μM), b) fluorescence emission (5 μM) spectra and c) color changes of **1** (5 μM) in different solvents. λ_{ex} = 470 nm, slit = 5 nm, 10 nm.

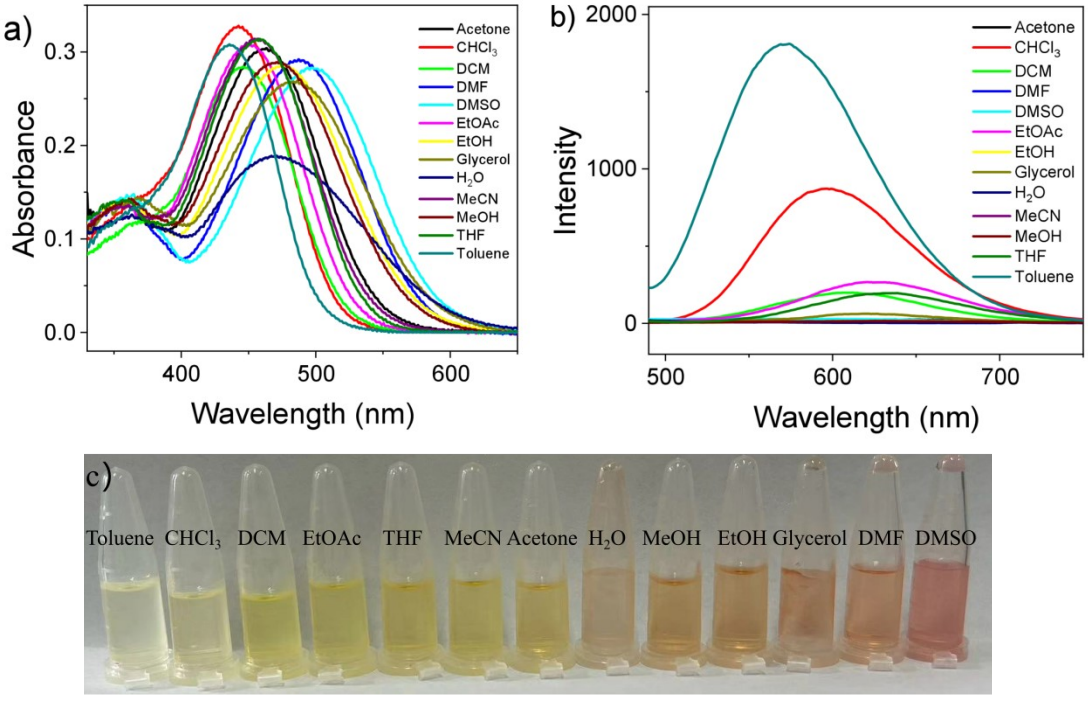

Fig. S2. a) UV/vis absorption (10 μM), b) fluorescence emission (5 μM) spectra and c) color changes of **2** (5 μM) in different solvents. λ_{ex} = 470 nm, slit = 5 nm, 10 nm.

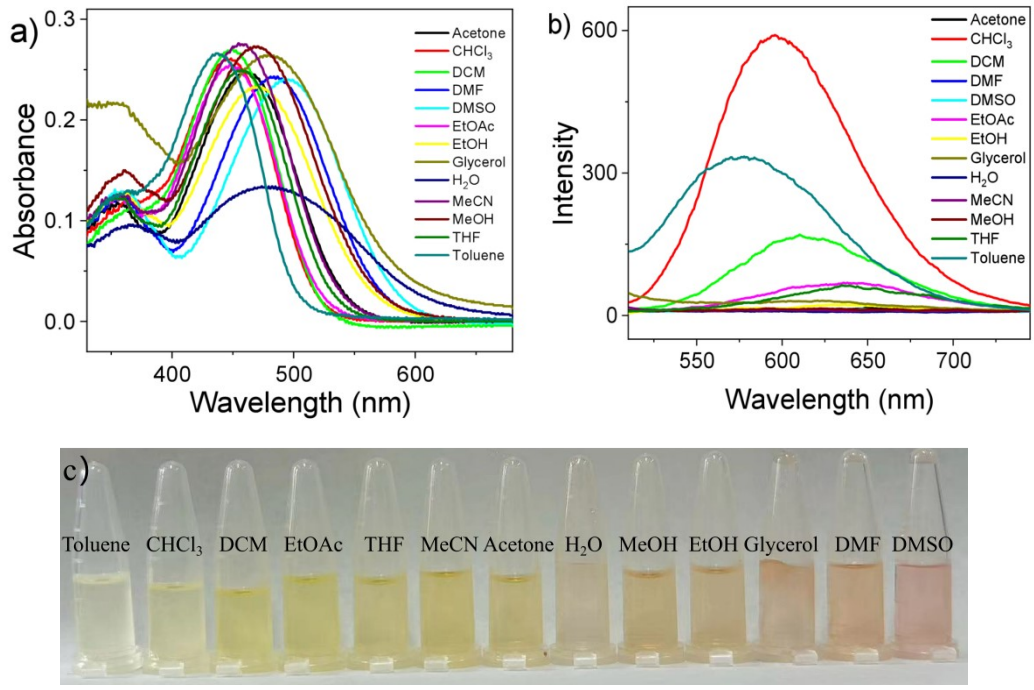

Fig. S3. a) UV/vis absorption (10 μM), b) fluorescence emission (5 μM) spectra and c) color changes of **3** (5 μM) in different solvents. λ_{ex} = 490 nm, slit = 5 nm, 10 nm.

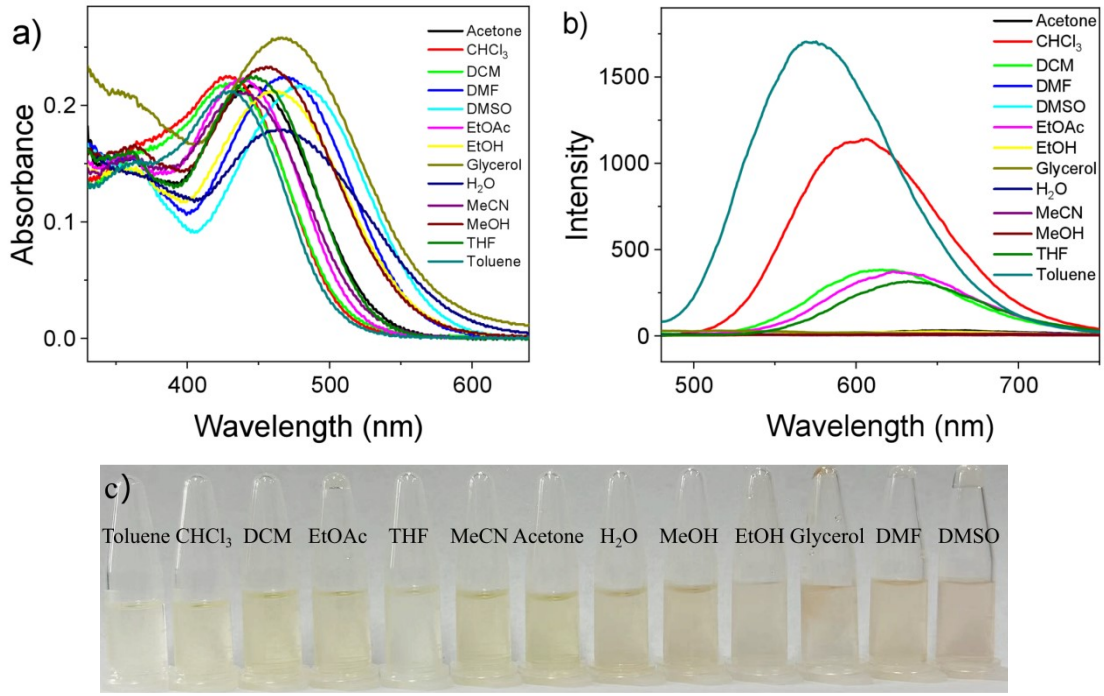

Fig. S4. a) UV/vis absorption (10 μM), b) fluorescence emission (5 μM) spectra and c) color changes of **4** (5 μM) in different solvents. λ_{ex} = 460 nm, slit = 5 nm, 10 nm.

Table S2. Chemical structures and spectroscopic data of probes **1-4** in ethanol.

Entry	Structures	substituents	$\lambda_{abs,max}$ (nm)	$\lambda_{em,max}$ (nm)	Stokes shift (nm)	ε ($M^{-1}cm^{-1}$)	Φ_f
1	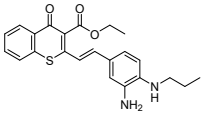	n-propyl	480	620	153	25200	0.0046
2	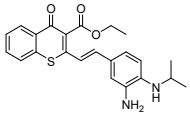	iso-propyl	480	620	153	28500	0.0023
3	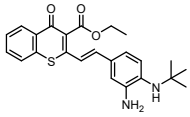	tert-butyl	472	621	149	23300	0.0027
4	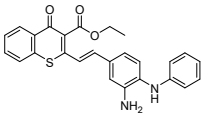	phenyl	464	651	187	21200	0.0022

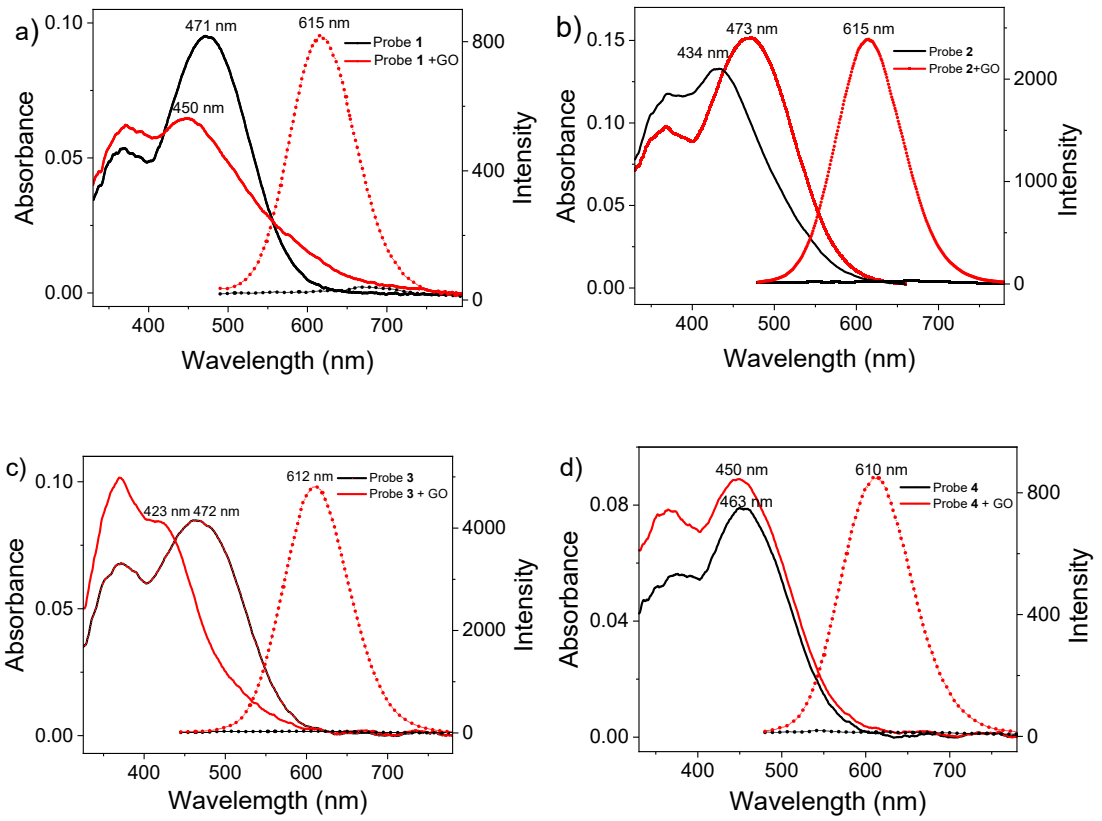

Fig. S5. The absorption spectra of probes **1-4** (5 μM) and fluorescence spectra of probes **1-4** (5 μM) and GO before and after the reaction in PBS-EtOH (2:1, v/v, pH 7.4) at 37 °C. a) **1** + GO **(**1000 equiv.), 2 h, λ_{ex} = 470 nm, slit = 10 nm, 10 nm; b) **2** + GO (1000 equiv.), 1.5 h, λ_{ex} = 460 nm, slit = 10 nm, 10 nm; c) **3** + GO **(**1000 equiv.), 1 h, λ_{ex} = 425 nm, slit = 10 nm, 10 nm; d) **4** + GO **(**4000 equiv.), 1 h, λ_{ex} = 460 nm, slit = 10 nm, 10 nm.

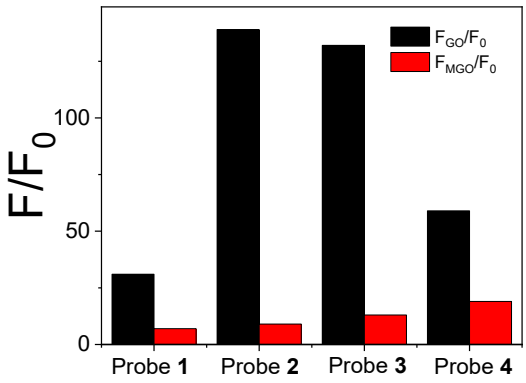

Fig. S6. Fluorescence intensity ratio of **1-4** (5 μM) reacted with GO (**1-3**: 5 mM; **4**: 20 mM) and MGO (**1-3**: 5 mM; **4**: 20 mM) in PBS-EtOH (2:1, v/v, pH 7.4) at 37 ℃ for 2 h. **1**: λ_{ex} = 470 nm, λ_{em} = 615 nm, slit = 10 nm, 10 nm; **2**: λ_{ex} = 460 nm, λ_{em} = 615 nm, slit = 10 nm, 10 nm; **3**: λ_{ex} = 425 nm, λ_{em} = 612 nm, slit = 10 nm, 10 nm; **4**: λ_{ex} = 460 nm, λ_{em} = 610 nm, slit = 10 nm, 10 nm.

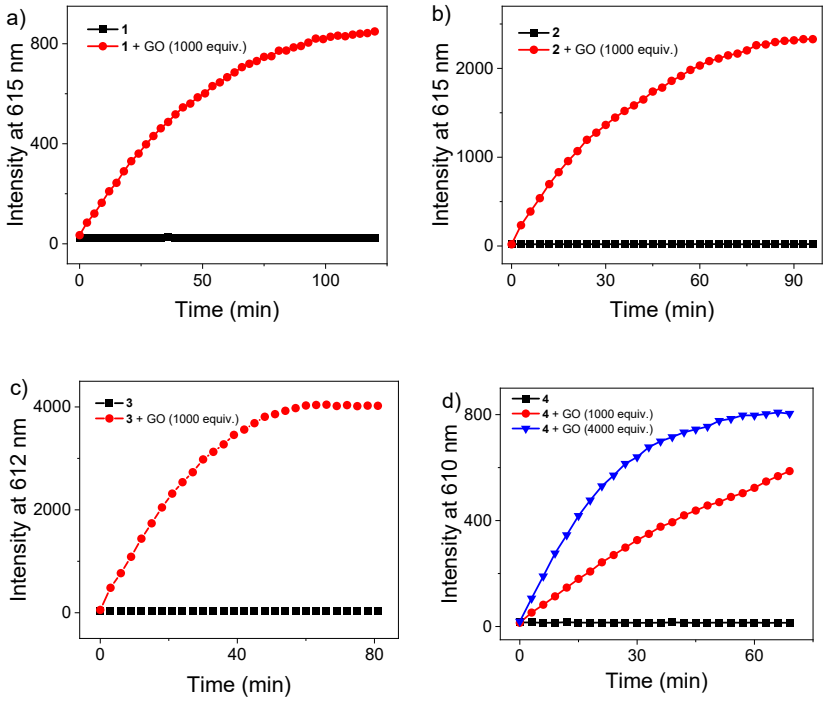

Fig. S7. Time-dependent fluorescence intensity of probe **1-4** (0.5 μM) upon the addition of GO in PBS-EtOH (2:1, v/v, pH 7.4). a) λ_{ex} = 470 nm, slit = 10 nm, 10 nm; b) λ_{ex} = 460 nm, slit = 10 nm, 10 nm; c) λ_{ex} = 425 nm, slit = 10 nm, 10 nm; d) λ_{ex} =

460 nm, slit = 10 nm, 10 nm.

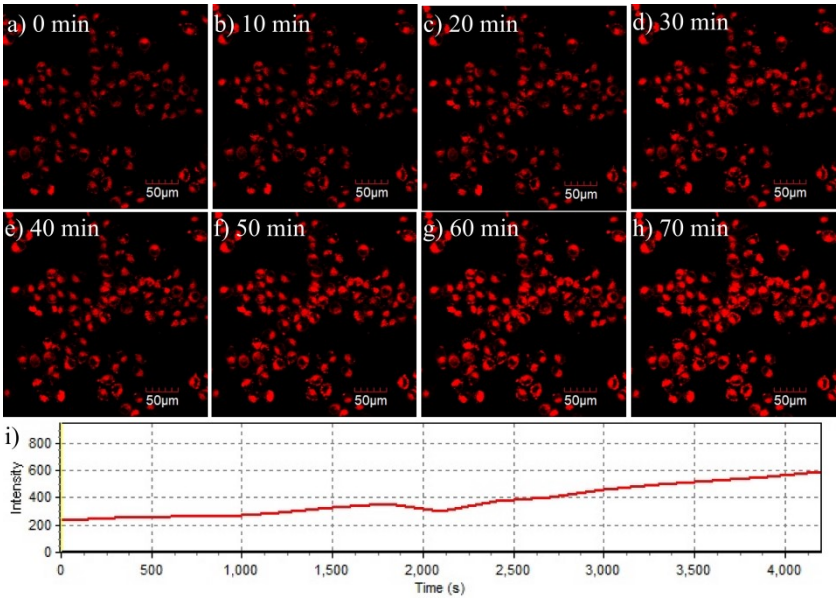

Fig. S8. Time-dependent confocal fluorescence imaging of the probe **1** in HeLa cells. (a-h) HeLa cells were incubated with the probe **1** (2 μM) for 20 min, then time-dependent imaging was carried out for 70 min, and the images were taken every 5 min for a total of 70 min; (i) The time-dependent fluorescence intensity changes of the probe **1** (2 μM) with continuous laser excitation. λ_{ex} = 488 nm, λ_{em} = 570-670 nm. Scale bar: 50 μm.

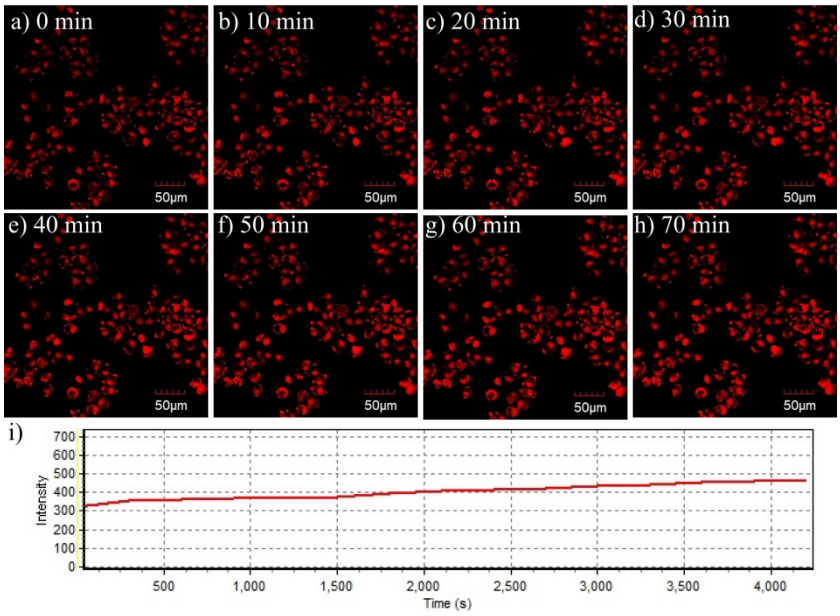

Fig. S9. Time-dependent confocal fluorescence imaging of the probe **2** in HeLa cells. (a-h) HeLa cells were incubated with the probe **2** (2 μM) for 20 min, then time-dependent imaging was carried out for 70 min, and the images were taken every 5 min for a total of 70 min; (i) The time-dependent fluorescence intensity changes of the probe **2** (2 μM) with continuous laser excitation. λ_{ex} = 488 nm, λ_{em} = 570-670 nm. Scale bar: 50 μm.

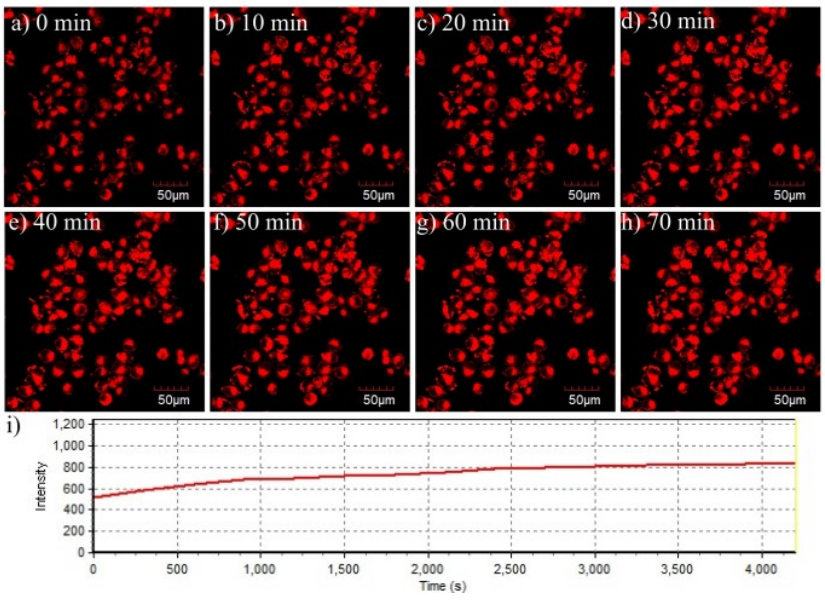

Fig. S10. Time-dependent confocal fluorescence imaging of the probe **3** in HeLa cells. (a-h) HeLa cells were incubated with the probe **3** (2 μM) for 20 min, then time-dependent imaging was carried out for 70 min, and the images were taken every 5 min for a total of 70 min; (i) The time-dependent fluorescence intensity changes of the probe **3** (2 μM) with continuous laser excitation. λ_{ex} = 488 nm, λ_{em} = 570-670 nm. Scale bar: 50 μm.

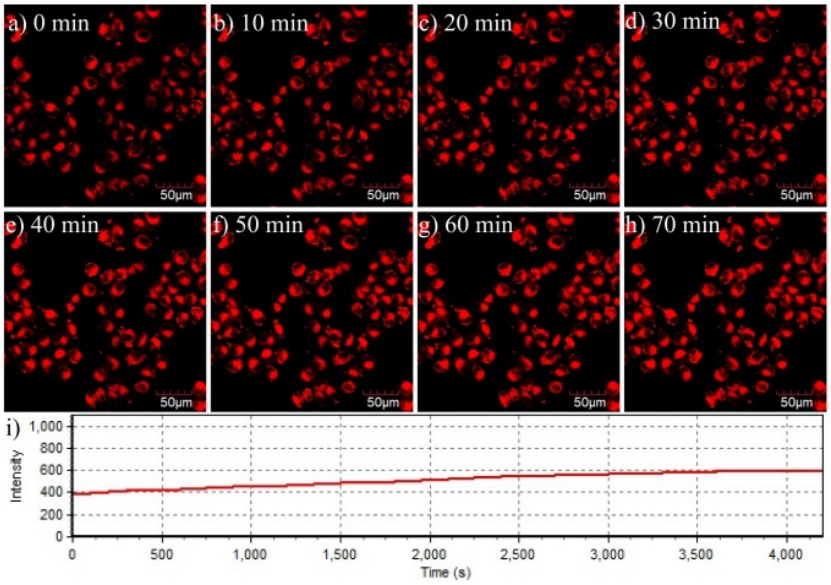

Fig. S11. Time-dependent confocal fluorescence imaging of the probe **4** in HeLa cells. (a-h) HeLa cells were incubated with the probe **4** (2 μM) for 20 min, then time-dependent imaging was carried out for 70 min, and the images were taken every 5 min for a total of 70 min; (i) The time-dependent fluorescence intensity changes of the probe **4** (2 μM) with continuous laser excitation. λ_{ex} = 488 nm, λ_{em} = 570-670 nm. Scale bar: 50 μm.

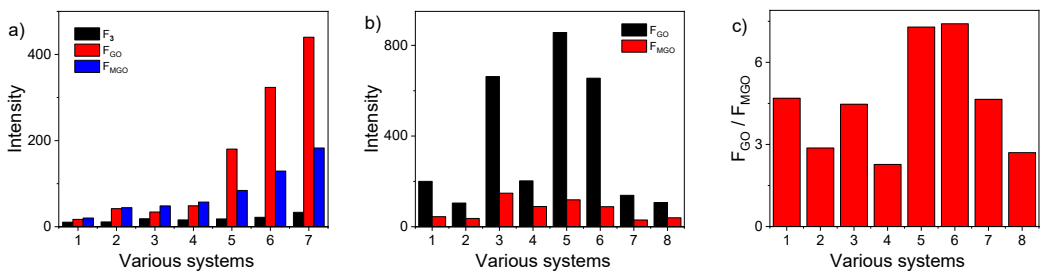

Fig. S12. a) Fluorescence intensity of **3** (5 μM) at 612 nm upon the addition of GO (5 mM) and MGO (5 mM) in different PBS with ethanol systems at room for 2 h. 1: PBS, 2: PBS:EtOH = 9:1, 3: PBS:EtOH = 5:1, 4: PBS:EtOH = 4:1, 5: PBS:EtOH = 3:1, 6: PBS: EtOH = 2:1, 7: PBS:EtOH = 1:1. b) The fluorescence intensity and c) fluorescence intensity ratio of **3** (5 μM) reacted with GO (5 mM) and MGO (5 mM) in different solvents at 37 °C for 2 h. 1: H_2O:EtOH = 1:1; 2: H_2O:EtOH = 2:1; 3: PBS:DMSO = 1:1; 4: PBS:DMSO = 2:1; 5: PBS:EtOH = 1:1; 6: PBS:EtOH = 2:1; 7: PBS:MeCN = 1:1; 8: PBS:MeCN = 2:1. λ_{ex} = 490 nm, slit = 10 nm, 10 nm.

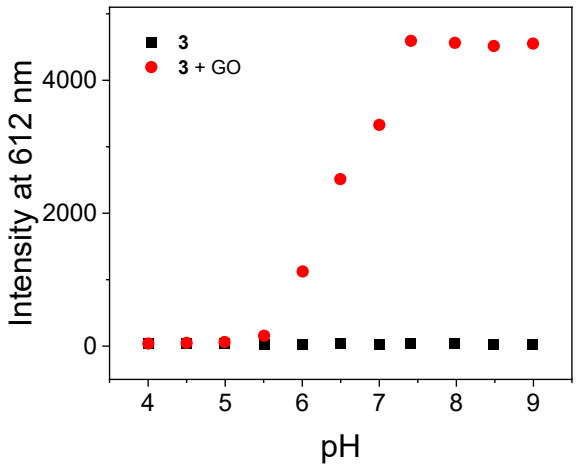

Fig. S13. Fluorescence responses of **3** (5 μM) and **3** + GO (5.0 mM) under different pH conditions. λ_{ex} = 425 nm, slit = 10 nm, 10 nm.

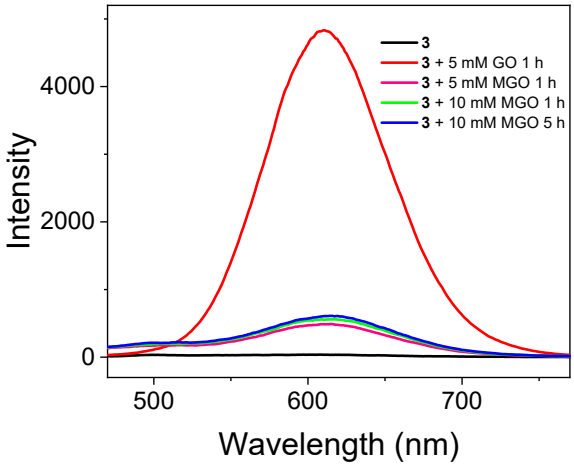

Fig. S14. Fluorescence response of **3** (5 μM) to the addition of GO and MGO. λ_{ex} = 425 nm, slit = 10 nm, 10 nm.

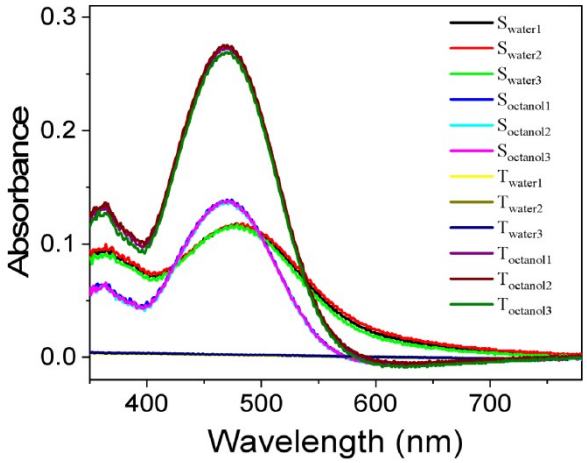

Fig. S15. The absorption spectra of probes **3** in water and octanol phase, S_{water} and $S_{octanol}$ denoted the standard absorption spectra of probe **3** (5 uM) in the aqueous and n-octanol phases, respectively; T_{water} and $T_{octanol}$ indicated the test absorption spectra of probe **3** in the aqueous and n-octanol phases after the distribution treatment, respectively. Each experiment was repeated for three times.

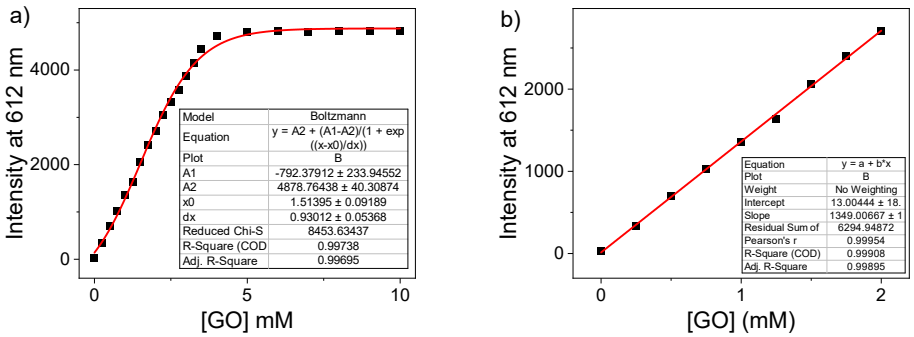

Fig. S16. a) Plot at 612 nm against GO concentration from 0 mM to 10 mM; b) Linear relationship of the fluorescence intensity at 612 nm against the concentration of GO from 0 mM to 2 mM. λ_{ex} = 425 nm, slit = 10 nm, 10 nm.

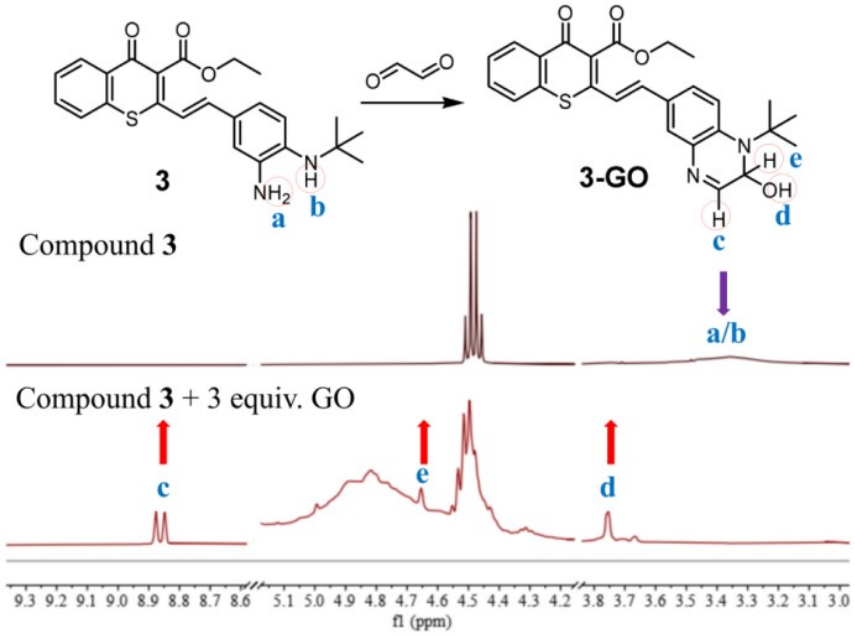

Fig. S17. The proposed mechanism of **3** with GO and ^{1}H NMR spectra of **3** in the presence of GO in $CDCl_3$ (400 MHz).

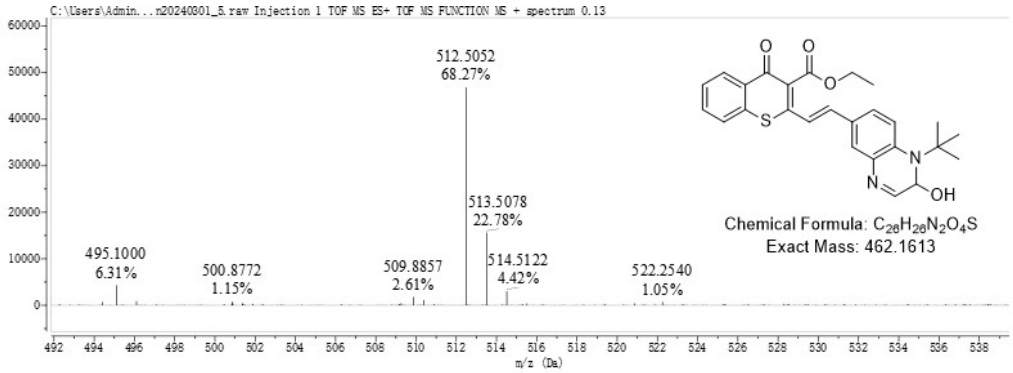

Fig. S18. HRMS (LC/MS) spectrum of **3-GO**. The peak at m/z = 512.5052 was assigned to the mass of [**3-GO** + MeOH + H_2O].

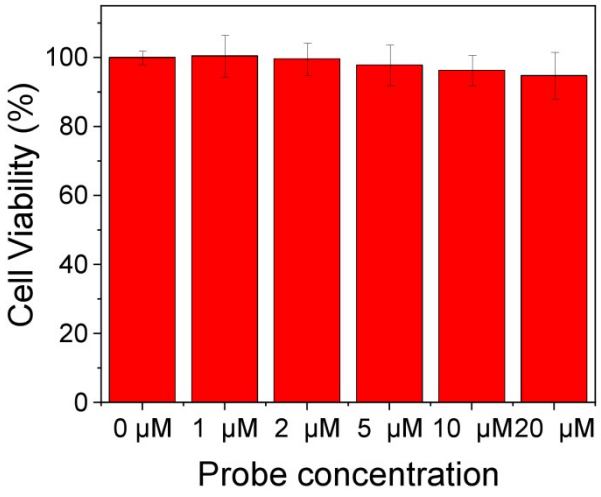

Fig. S19. Cytoxicity assay of **3** in HeLa cells. The cells were incubated with various concentrations of **3** (0, 1, 2, 5, 10 and 20 μM) over 24 h, respectively. The experiments were repeated three times.

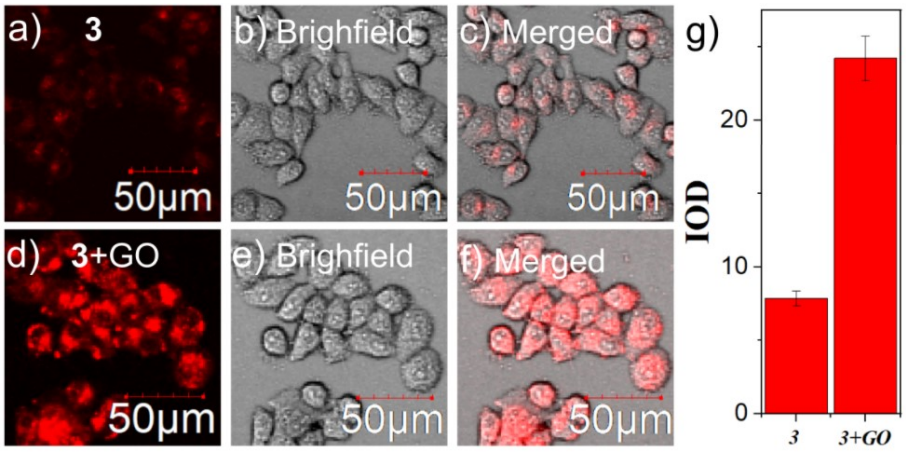

Fig. S20. Confocal fluorescence images of exogenous GO in HeLa cells. a-c) Hela cells were incubated with **3** (0.5 μM) for 1 h; d-f) Cells were incubated with **3** (0.5 μM) and GO (0.5 mM) for 1 h; g) Quantification of fluorescence intensities of corresponding a) and d). λ_{ex} = 488 nm, λ_{em} = 570-670 nm. Scale bar: 50 μm.

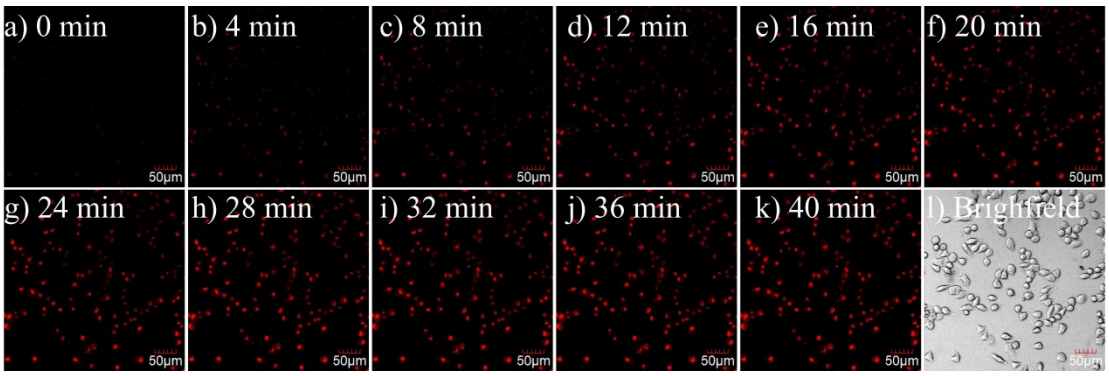

Fig. S21. Time-dependent confocal fluorescence imaging of the exogenous GO in HeLa cells. HeLa cells were incubated with the probe **3** (0.5 μM) for 60 min, GO (0.5 mM) added and the images were taken every 4 min for a total of 40 min. λ_{ex} = 488 nm, λ_{em} = 570-670 nm. Scale bar: 50 μm.

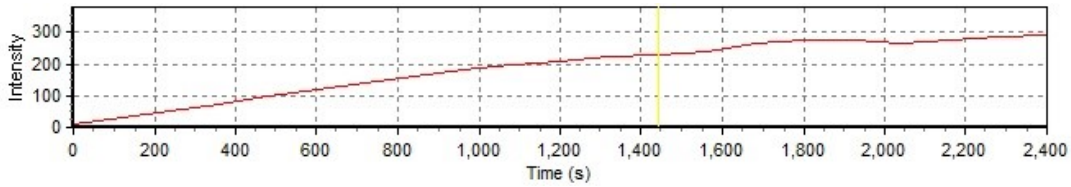

Fig. S22. The time-dependent fluorescence intensity changes of the probe **3** (0.5 μM) upon incubation with GO (0.5 mM) with continuous laser excitation.

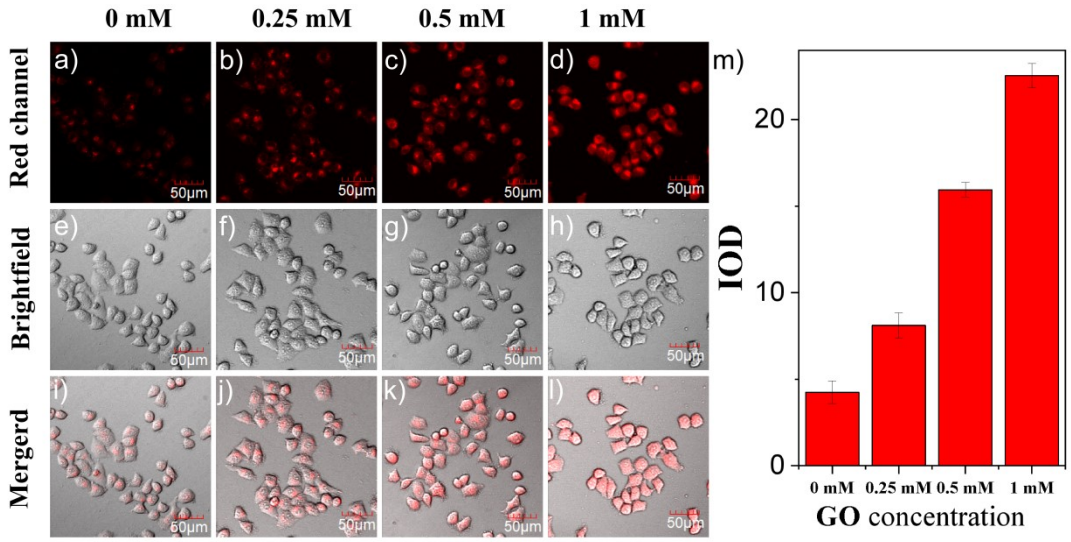

Fig. S23. Confocal fluorescence imaging of HeLa cells incubated with **3** being treated with different concentrations of glyoxal. (a-d) HeLa cells were incubated with **3** (0.5 μM) for 1 h and different levels of GO (0 μM, 0.25 mM, 0.5 mM and 1 mM) for another 1 h; (e-h) Corresponding brightfield; (i-l) Corresponding merged image; (m) Quantification of fluorescence intensities of corresponding (a-d). λ_{ex} = 488 nm, λ_{em} = 570-670 nm. Scale bar: 50 μm.

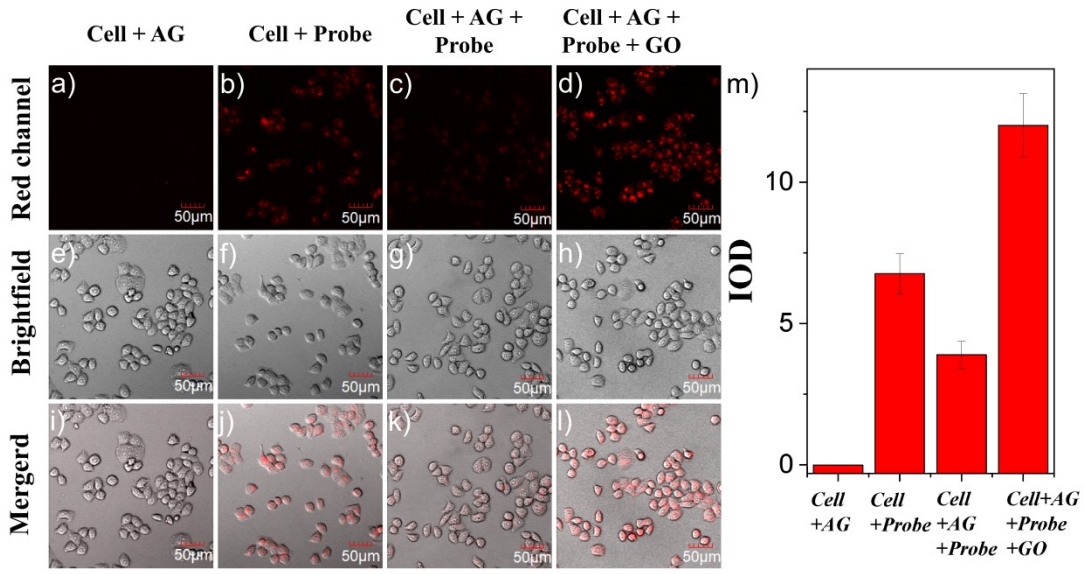

Fig. S24. Confocal fluorescence images of endogenous GO in HeLa cells. (a) HeLa cells were incubated with AG (5 mM) for 1 h; (b) HeLa cells were incubated with **3** (0.5 μM) for 1 h; (c) Cells were pre-incubated with AG (5 mM) for 1 h and then stained with **3** (0.5 μM) for another 1 h; (d) Cells were pre-incubated with AG (5 mM) for 1 h, stained with **3** (0.5 μM) for 1 h, then incubated with GO (0.5 mM) for 1 h; (e-h) Corresponding brightfield; (i-l) Corresponding merged image; (m) Quantification of fluorescence intensities of corresponding (a-d). λ_{ex} = 488 nm, λ_{em} = 570-670 nm. Scale bar: 50 μm.

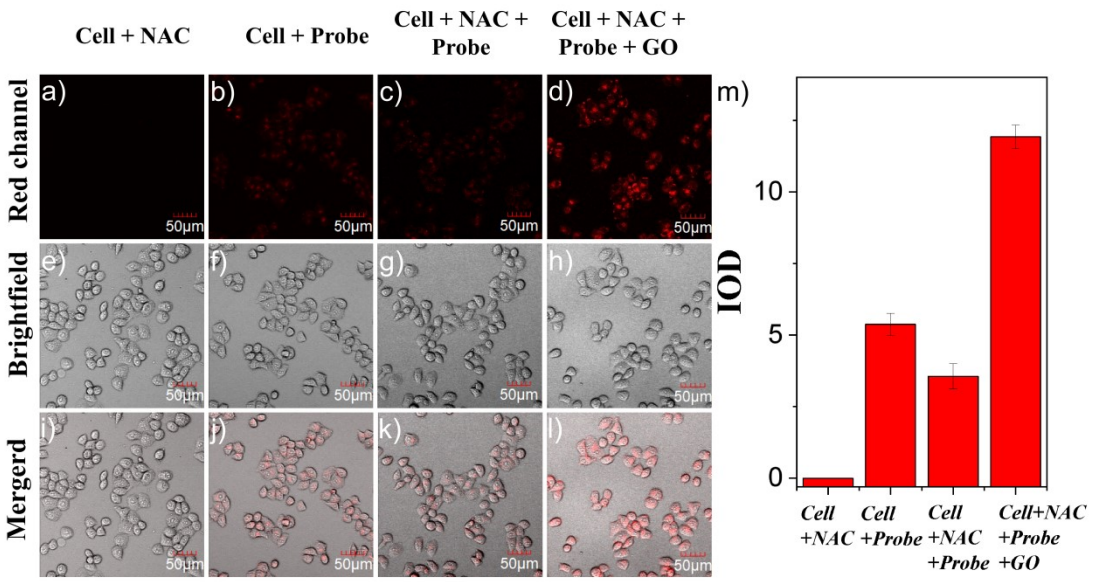

Fig. S25. Confocal fluorescence images of endogenous GO in HeLa cells. (a) HeLa cells were incubated with NAC (5 mM) for 1 h; (b) HeLa cells were incubated with **3** (0.5 μM) for 1 h; (c) Cells were pre-incubated with NAC (5 mM) for 1 h and then stained with **3** (0.5 μM) for another 1 h; (d) Cells were pre-incubated with NAC (5 mM) for 1 h, stained with **3** (0.5 μM) for 1 h, then incubated with GO (0.5 mM) for 1 h; (e-h) Corresponding brightfield; (i-l) Corresponding merged image; (m) Quantification of fluorescence intensities of corresponding (a-d). λ_{ex} = 488 nm, λ_{em} = 570-670 nm. Scale bar: 50 μm.

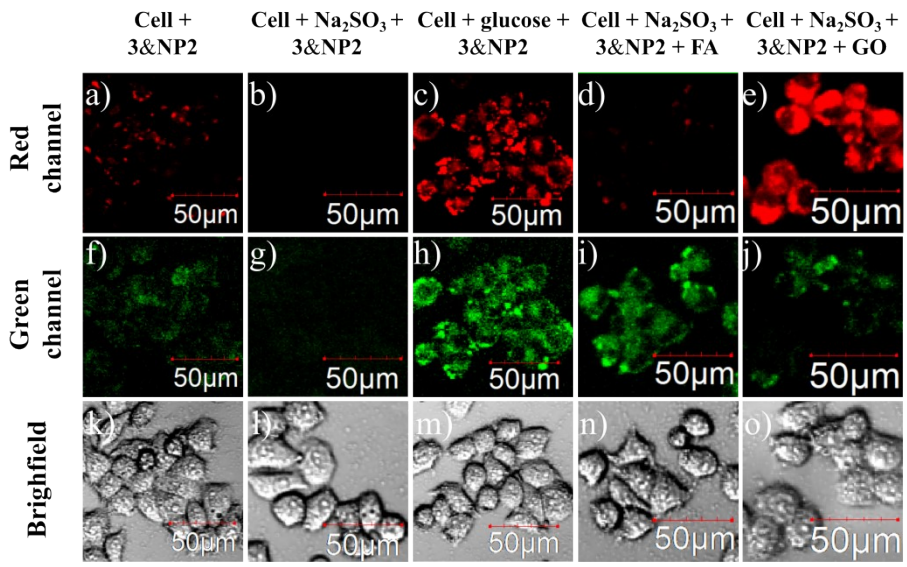

Fig. S26. Fluorescence images of living HeLa cells being incubated with **3** (1 μM) and **NP2** (3 μM). a) The cells were incubate with **3** and **NP2** for 1 h; b) The cells were pre-incubated with Na_2SO_3 (0.2 mM) for 1 h, then incubated with **3** and **NP2** for 1 h; c) The cells were pre-incubated with glucose (5 mM) for 12 h, then incubated with **3** and **NP2** for 1 h; d) The cells were pre-incubated with Na_2SO_3 (0.2 mM) for 1 h, stained with **3** and **NP2** for 1 h and then incubated with FA (3 mM) for 1 h; e) The cells were pre-incubated with Na_2SO_3 (0.2 mM) for 1 h, stained with **3** and **NP2** for 1 h and then incubated with GO (1 mM) for 1 h; (a-e) Corresponding red channel image; (f-j) Corresponding green channel image; (h-l) Corresponding brightfield image. Green channel: λ_{ex} = 405 nm, λ_{em} = 435-535 nm; Red channel: λ_{ex} = 559 nm, λ_{em} = 570-670 nm; Scale bar: 50 μm.

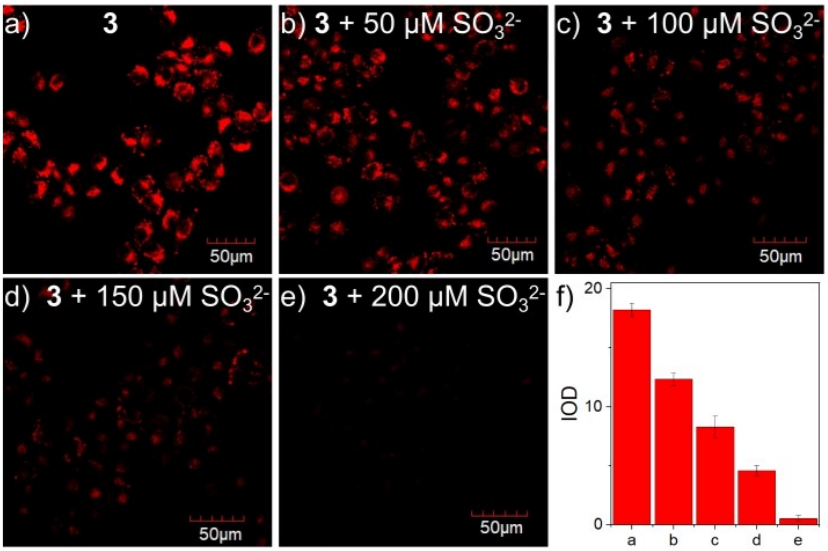

Fig. S27. Confocal fluorescence imaging of HeLa cells incubated with **3** being treated with different concentrations of SO_3^{2-}. (a-e) HeLa cells were incubated with different levels of GO (0 μM, 50 μM, 100 μM, 150 μM and 200 μM) for 30 min and then stained with **3** (3 μM) for 1 h; (f) Quantification of fluorescence intensities of corresponding (a-e). λ_{ex} = 488 nm, λ_{em} = 570-670 nm. Scale bar: 50 μm.

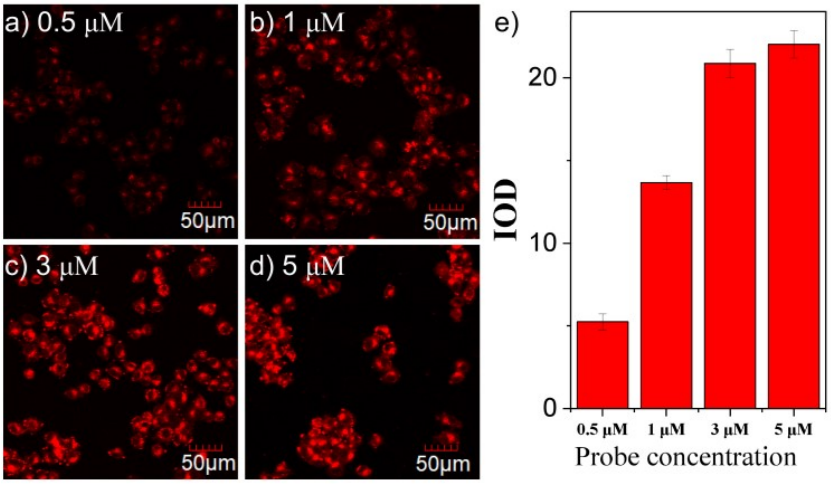

Fig. S28. Confocal fluorescence images of **3** in HeLa cells. (a-d) HeLa cells were incubated with different concentrations of **3** (0.5 μM, 1 μM, 3 μM, 5 μM) for 1 h, respectively. (e) Quantification of fluorescence intensities of corresponding (a-d). λ_{ex} = 488 nm, λ_{em} = 570-670 nm. Scale bar: 50 μm.

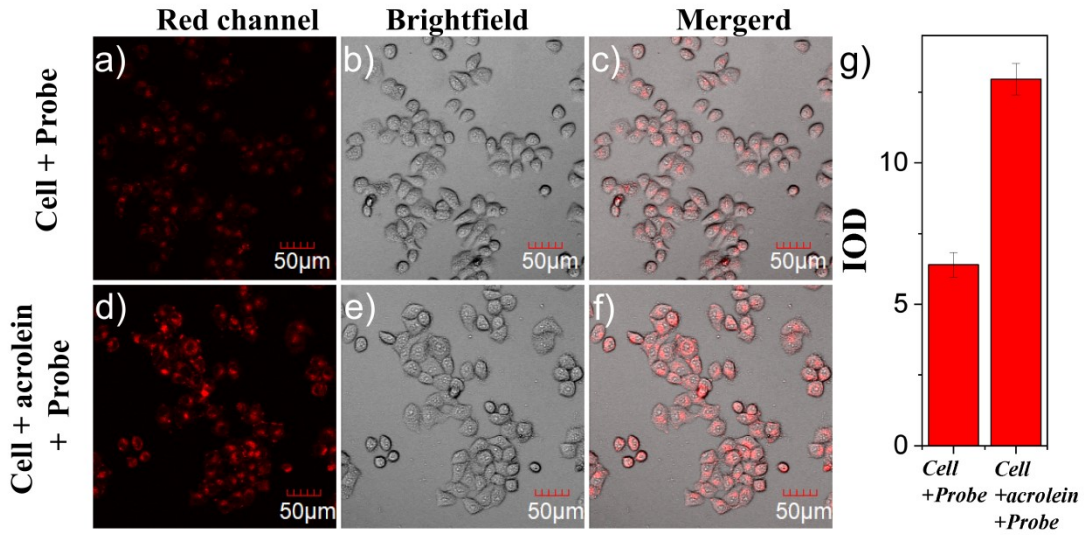

Fig. S29. Confocal fluorescence images of **3** for glyoxal during carbonyl stress. (a-c) HeLa cells were incubated with **3** (0.5 μM) for 1 h; (d-f) Cells were pre-incubated with acrolein (0.2 mM) for 2 h and then stained with **3** (0.5 μM) for another 1 h; (g) The relative fluorescence intensity of the cell output of group. λ_{ex} = 488 nm, λ_{em} = 570-670 nm. Scale bar: 50 μm.

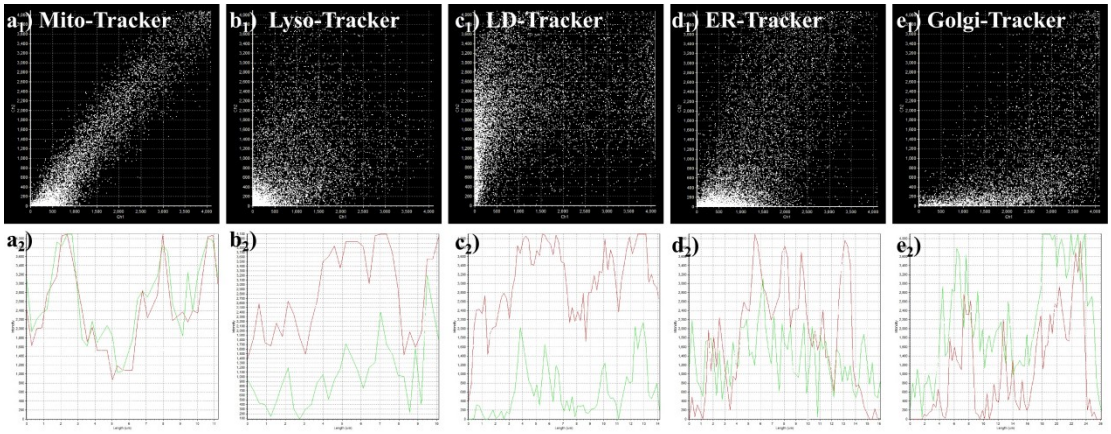

Fig. S30. Co-staining imaging of **3** and organelle trackers in HeLa cells. (a_1-e_1) Intensity correlation plot of **3** and organelle trackers, respectively; (a_2-e_2) Intensity profiles of **3** and organelle trackers within the linear ROI in Fig. 6 across the HeLa cell.

9. Optimized structures and computed total energies of probe 3 and 3-GO

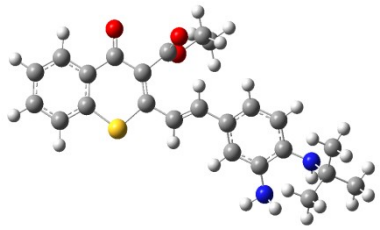

Fig. S31. Optimized structures of probe **3**.

B3LYP/6-31G (d,p)

Charge = 0 Multiplicity = 1

C	7.33066200	-1.43975500	-0.38623500
C	6.83546300	-2.69007500	0.01168500
C	5.47603600	-2.86928700	0.22369900
C	4.58904100	-1.79453700	0.03857900
C	5.07213200	-0.53738800	-0.36046900
C	6.45534000	-0.38115600	-0.56671100
S	2.87803500	-2.12764700	0.30430000
C	2.07857800	-0.57080700	0.05336100
C	2.76348100	0.55647300	-0.30552900
C	4.20590100	0.65383200	-0.56036100
O	4.69394300	1.73198100	-0.91367100
C	2.07873100	1.89551700	-0.44394700
O	2.24562000	2.62870200	0.66796200
O	1.47559300	2.27603600	-1.42532700

C	1.73683900	3.98341400	0.61117700
C	2.07156700	4.64817300	1.93195100
C	0.64369900	-0.70288600	0.30508900
C	-0.34413600	-0.05679800	-0.36047000
C	-1.77502000	-0.19099900	-0.13560800
C	-2.33853100	-0.91182600	0.94022700
C	-3.70839500	-1.02575200	1.10455900
C	-4.60362600	-0.42014300	0.16736200
C	-4.04209300	0.33433100	-0.87482300
C	-2.66182800	0.44517100	-1.01739200
N	-5.95585000	-0.61620900	0.41084100
N	-4.28817200	-1.77315700	2.15897300
C	-7.10164600	-0.26196600	-0.45334200
C	-8.34149700	-0.83003800	0.26216200
C	-7.00145800	-0.90029400	-1.85584400
C	-7.25464200	1.26878000	-0.54191400
H	8.39472300	-1.30297400	-0.55191200
H	7.51410700	-3.52544300	0.15662800
H	5.09270300	-3.83771500	0.53201700
H	6.79936200	0.60087700	-0.87207700
H	0.65824500	3.94735500	0.42803400
H	2.20203500	4.49296300	-0.23771800

H	1.70495100	5.67948700	1.93174000
H	3.15264100	4.66589000	2.09467700
H	1.60548500	4.11723500	2.76699400
H	0.38174400	-1.44960200	1.05240600
H	-0.06537100	0.61860200	-1.16356400
H	-1.69188200	-1.37370600	1.68197800
H	-4.67871800	0.82683700	-1.59646800
H	-2.26146600	1.02663100	-1.84297200
H	-6.10284300	-1.48144700	0.92034900
H	-4.93699400	-1.21423700	2.70859400
H	-3.59024900	-2.17366600	2.77525900
H	-9.24957300	-0.58963800	-0.29719000
H	-8.43516600	-0.40998900	1.26852200
H	-8.28219500	-1.92157700	0.34658100
H	-7.88668000	-0.65307600	-2.45110600
H	-6.94075300	-1.99038400	-1.77462600
H	-6.12216300	-0.55856800	-2.40532700
H	-8.16148700	1.52051600	-1.10072300
H	-6.41346300	1.75028300	-1.04358100
H	-7.33622400	1.69759700	0.46103000

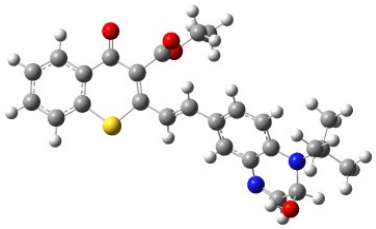

Fig. S32. Optimized structures of compound **3-GO**.

B3LYP/6-31G (d,p)

Charge = 0 Multiplicity = 1

C	7.81518400	-1.53498700	-0.39253100
C	7.27540200	-2.79391100	-0.09102200
C	5.90712400	-2.94618700	0.08064800
C	5.05592800	-1.83488800	-0.04805500
C	5.58370700	-0.56860300	-0.35064900
C	6.97521200	-0.44064600	-0.51821000
S	3.33102900	-2.13444200	0.16268200
C	2.58484100	-0.54233300	-0.00237700
C	3.30556300	0.58663700	-0.26806300
C	4.75712100	0.65828700	-0.48791700
O	5.28037200	1.74198600	-0.76276400
C	2.65826600	1.95015100	-0.32982500
O	2.83794700	2.60928900	0.82422800
O	2.07137400	2.40370400	-1.29009700
C	2.36777300	3.97947400	0.84913600
C	2.70910600	4.55002400	2.21146000

C	1.13732700	-0.64462300	0.20692900
C	0.19291600	0.04970600	-0.46695100
C	-1.25142500	-0.05452000	-0.28821100
C	-1.87280000	-0.82180000	0.70532000
C	-3.25897900	-0.89862700	0.82517800
C	-4.12001600	-0.17173500	-0.05722500
C	-3.48434100	0.60349400	-1.05132400
C	-2.10157100	0.65671300	-1.15570900
N	-5.50017200	-0.26374000	0.14614400
N	-3.75644800	-1.69160600	1.86581800
C	-6.50470100	0.58375000	-0.59521100
C	-6.19166100	2.08028200	-0.37489900
C	-5.97568400	-1.46986200	0.79849300
C	-5.01551100	-1.92010200	1.86888700
O	-6.26067300	-2.54912900	-0.10668300
C	-7.92110300	0.36033000	-0.02242500
C	-6.56355800	0.19364300	-2.09082400
H	8.88615400	-1.41962500	-0.52668400
H	7.92638400	-3.65717700	0.01038200
H	5.48948500	-3.92122300	0.31439300
H	7.35444300	0.54865000	-0.74933900
H	1.29033800	3.98507700	0.65633100

H	2.85501800	4.52704300	0.03711200
H	2.37149000	5.58931900	2.27319000
H	3.78871500	4.52679800	2.38274500
H	2.22064300	3.98142800	3.00793000
H	0.83304100	-1.40267200	0.92627900
H	0.51566100	0.74803700	-1.23318200
H	-1.30007600	-1.38549800	1.43409500
H	-4.06122900	1.16494400	-1.76854600
H	-1.66310600	1.26461800	-1.94247700
H	-6.92999800	2.68578300	-0.90899200
H	-5.20487400	2.38511200	-0.71798600
H	-6.26006100	2.32103000	0.69016700
H	-6.93763800	-1.27296500	1.26245800
H	-5.43182200	-2.53097700	2.67060400
H	-5.41814200	-2.85715500	-0.47188700
H	-8.60036600	1.04992300	-0.53025900
H	-7.97052600	0.58312500	1.04809300
H	-8.29166200	-0.65209300	-0.20009800
H	-7.33356900	0.78315300	-2.59898300
H	-6.82209300	-0.86459200	-2.17829800
H	-5.62320700	0.35363400	-2.61889000

10. Structural characterizations

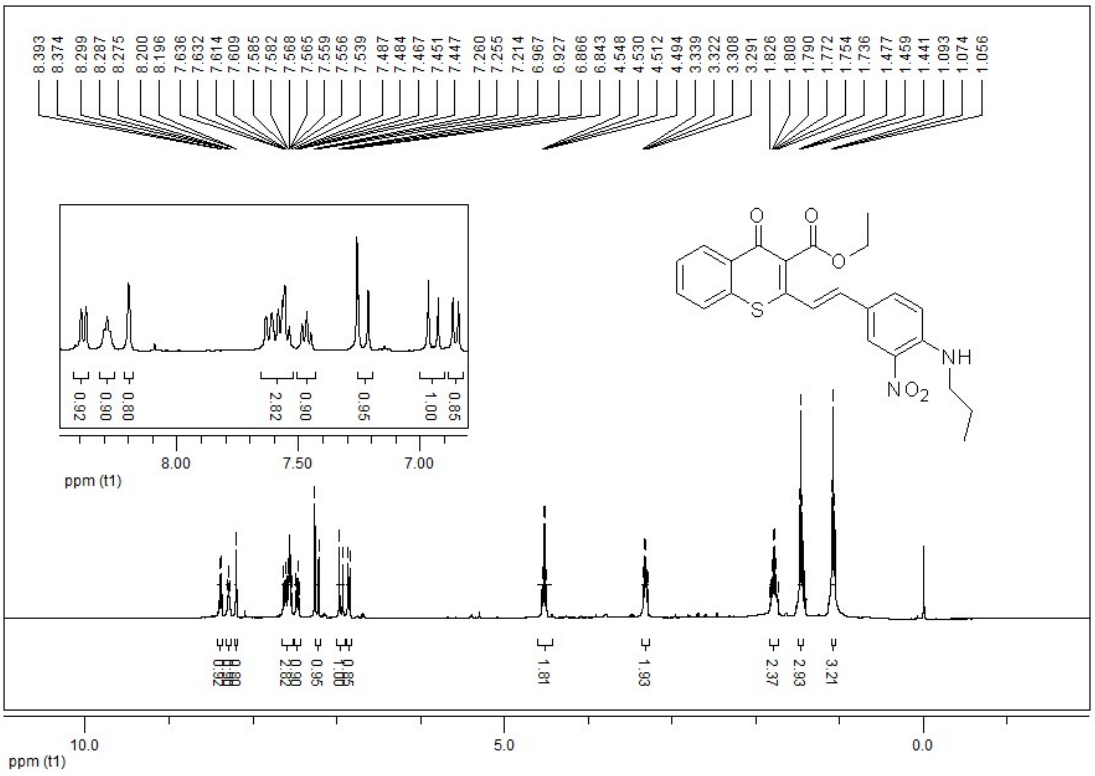

Fig. S33. ^{1}H NMR spectrum of compound **a** (400 MHz, $CDCl_3$)

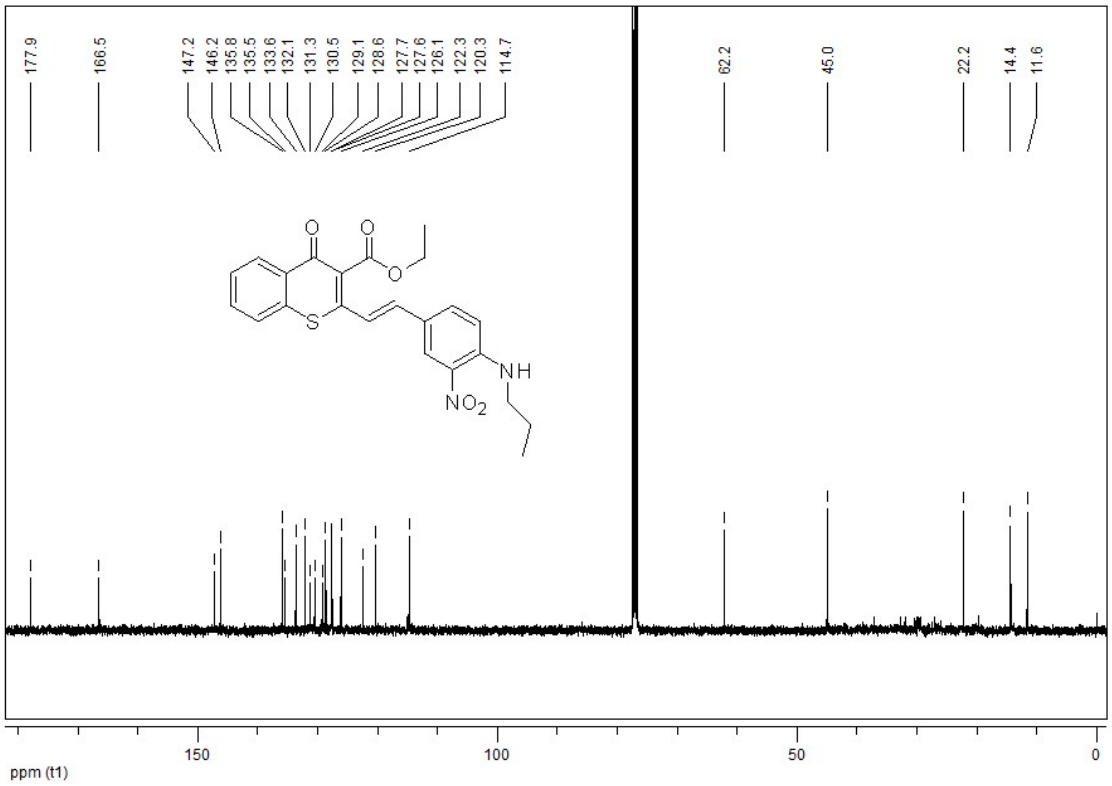

Fig. S34. ^{13}C NMR spectrum of compound **a** (100 MHz, $CDCl_3$)

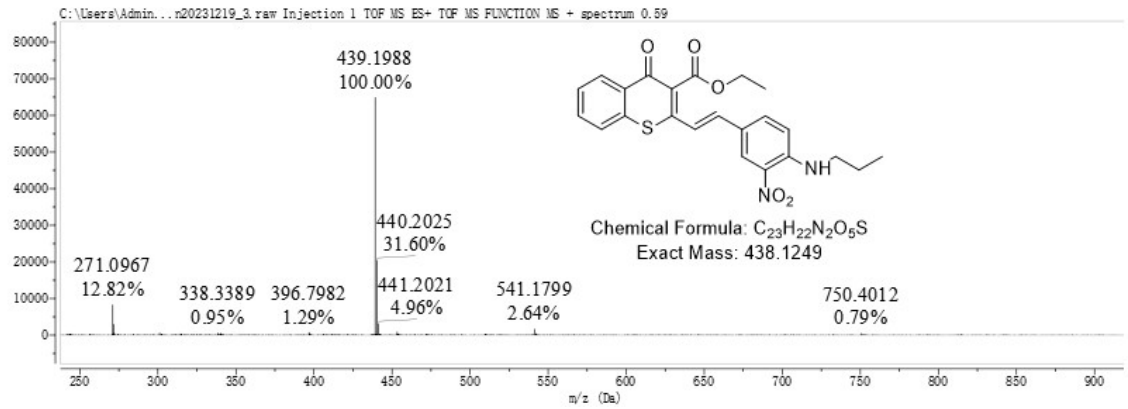

Fig. S35. HRMS (LC/MS) spectrum of **a**. The peak at m/z = 439.1988 was assigned to the mass of [**a** + H^+].

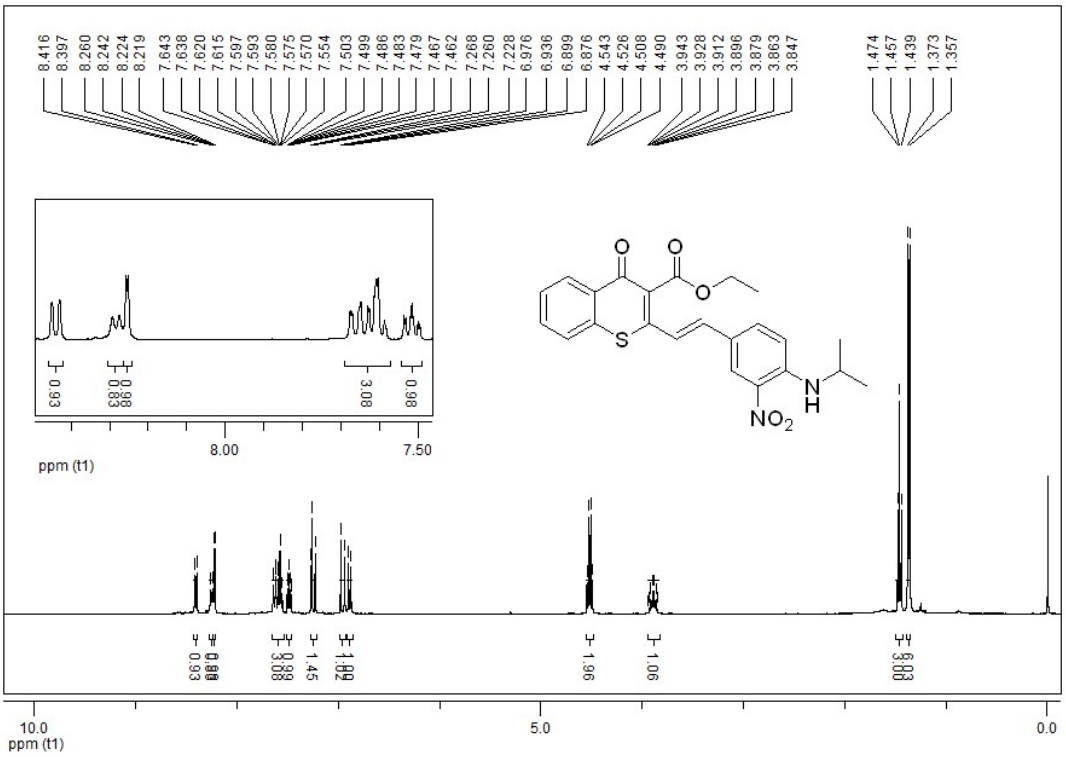

Fig. S36. ^{1}H NMR spectrum of compound **b** (400 MHz, $CDCl_3$)

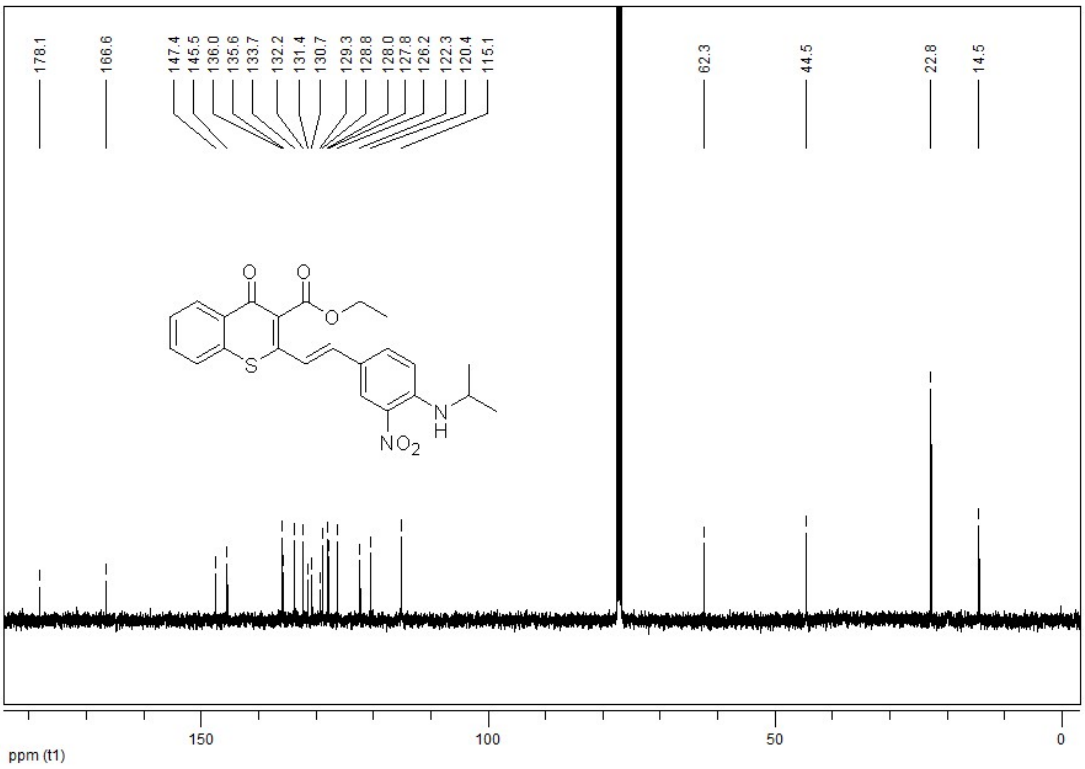

Fig. S37. ^{13}C NMR spectrum of compound **b** (100 MHz, $CDCl_3$)

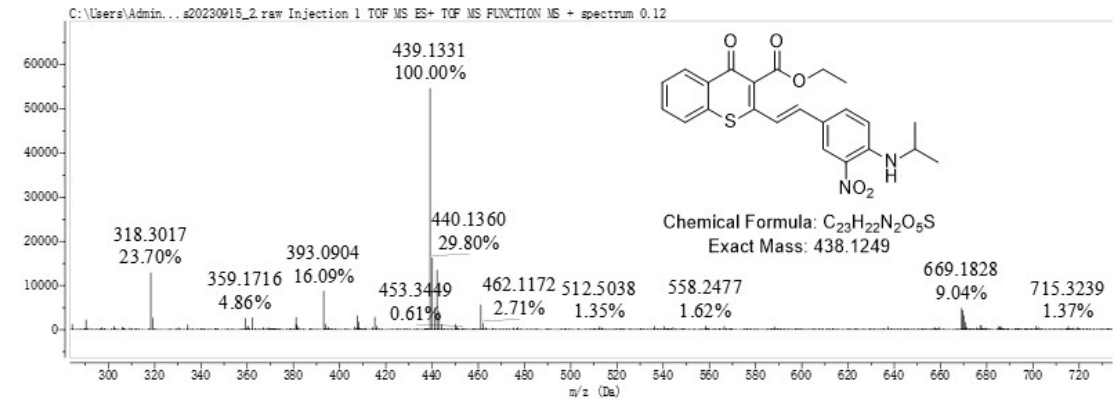

Fig. S38. HRMS (LC/MS) spectrum of **b**. The peak at m/z = 439.1331 was assigned to the mass of [**b** + H^+].

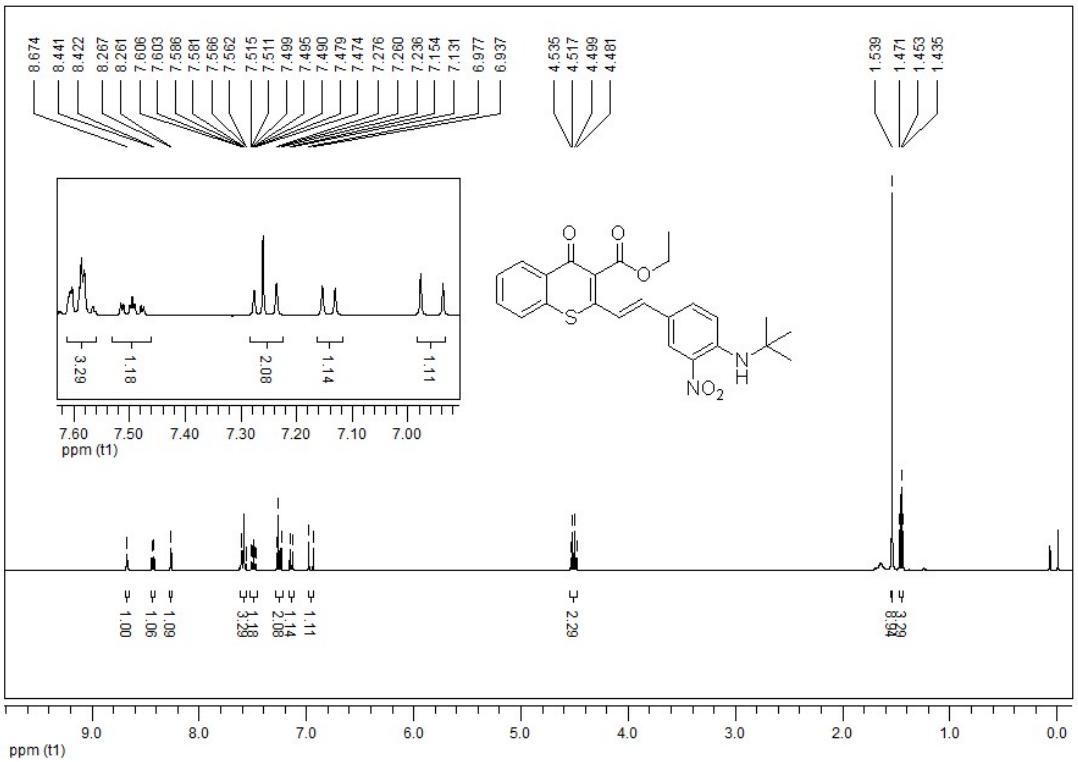

Fig. S39. ^{1}H NMR spectrum of compound **c** (400 MHz, $CDCl_3$)

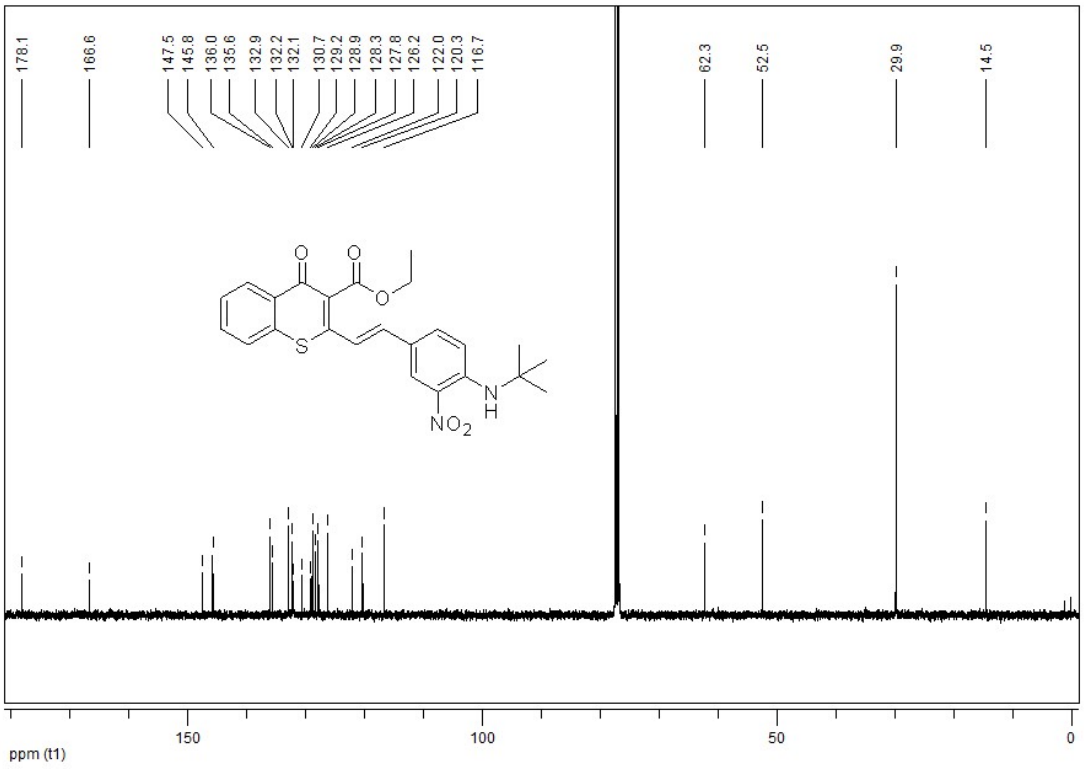

Fig. S40. ^{13}C NMR spectrum of compound **c** (100 MHz, $CDCl_3$)

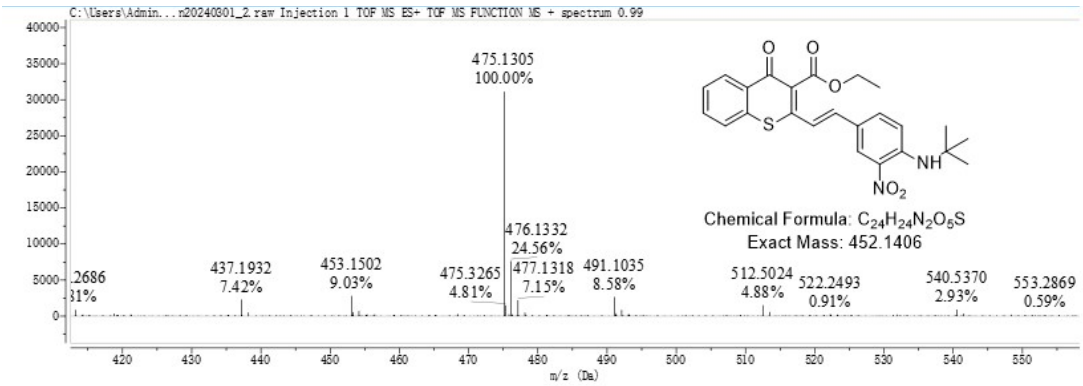

Fig. S41. HRMS (LC/MS) spectrum of **c**. The peak at m/z = 475.1305 was assigned to the mass of [**c** + Na^+].

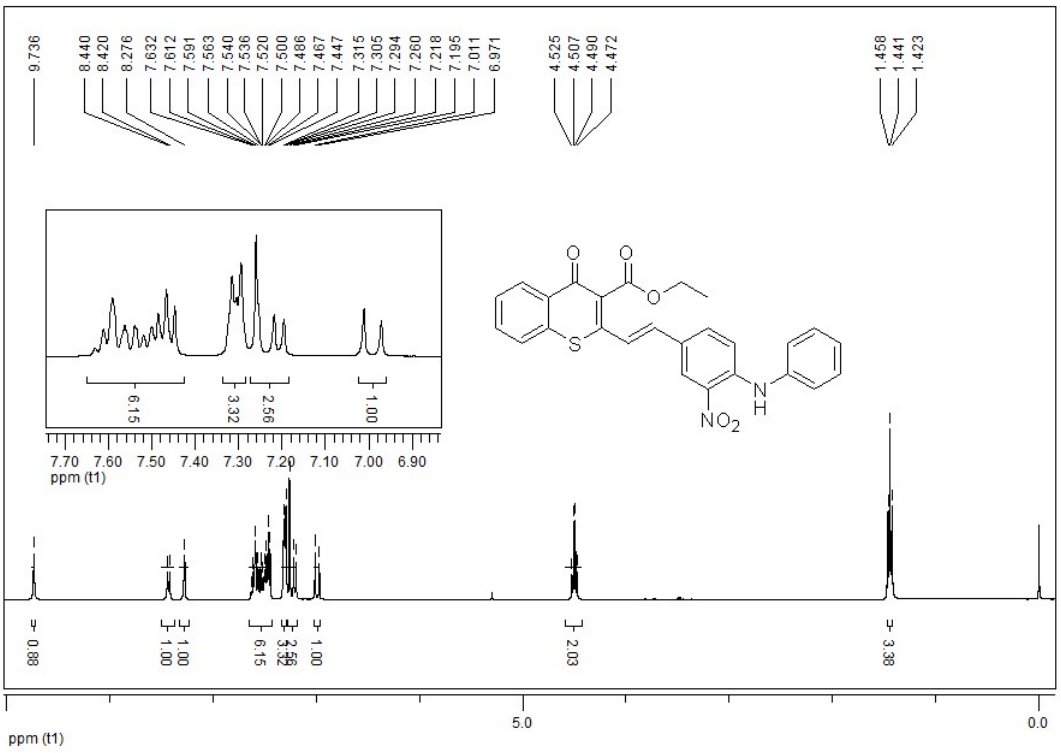

Fig. S42. ^1H NMR spectrum of compound **d** (400 MHz, $CDCl_3$)

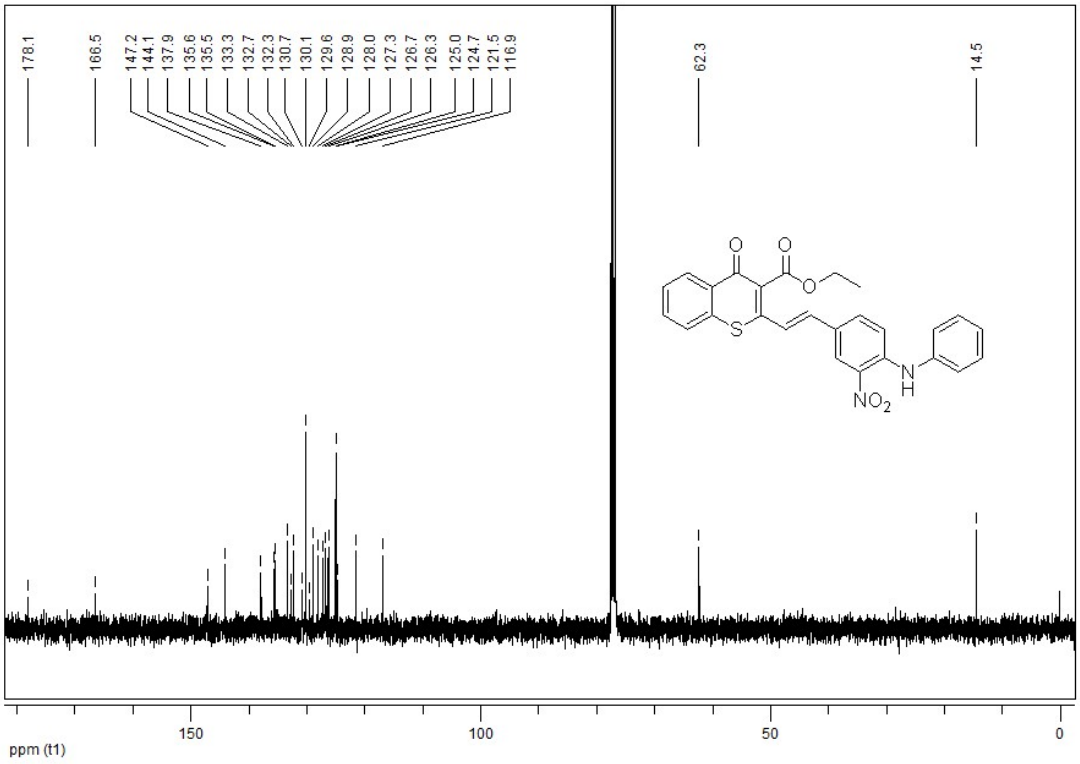

Fig. S43. ^{13}C NMR spectrum of compound **d** (100 MHz, $CDCl_3$)

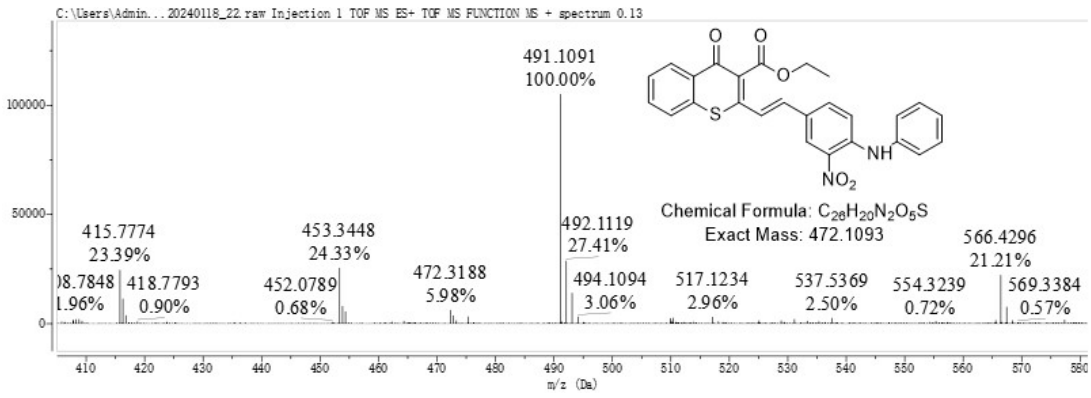

Fig. S44. HRMS (LC/MS) spectrum of **d**. The peak at m/z = 491.1091 was assigned to the mass of [**d** + H^+ + H_2O].

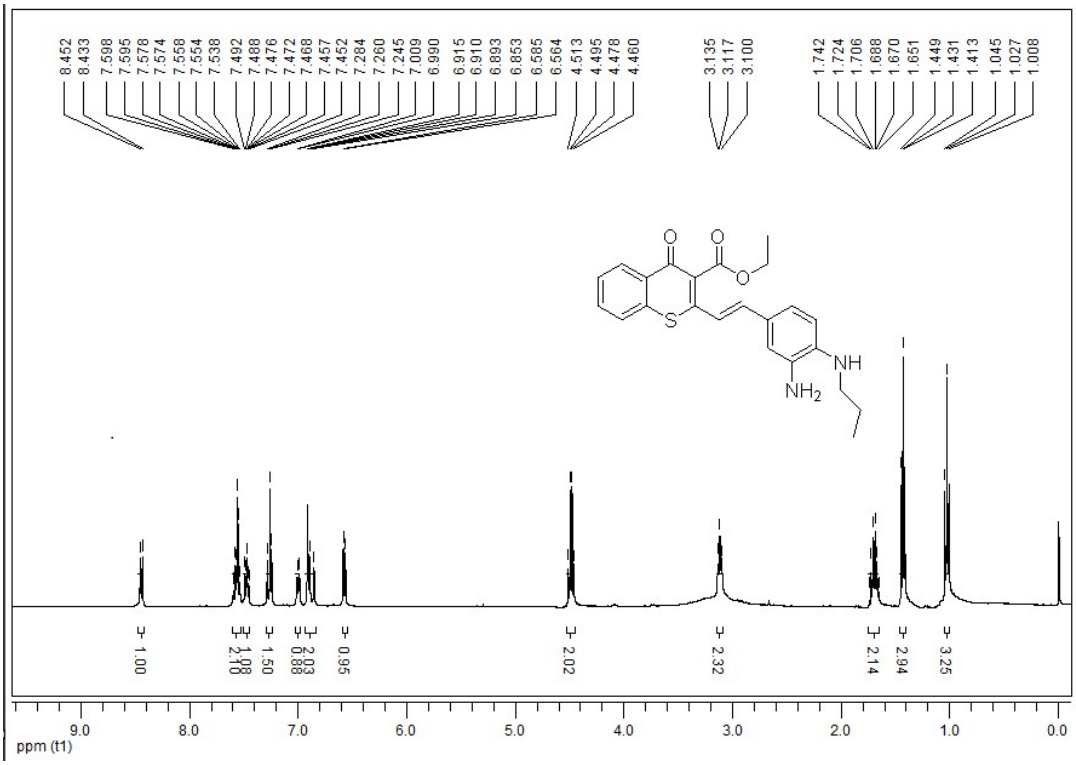

Fig. S45. ^{1}H NMR spectrum of compound **1** (400 MHz, $CDCl_3$)

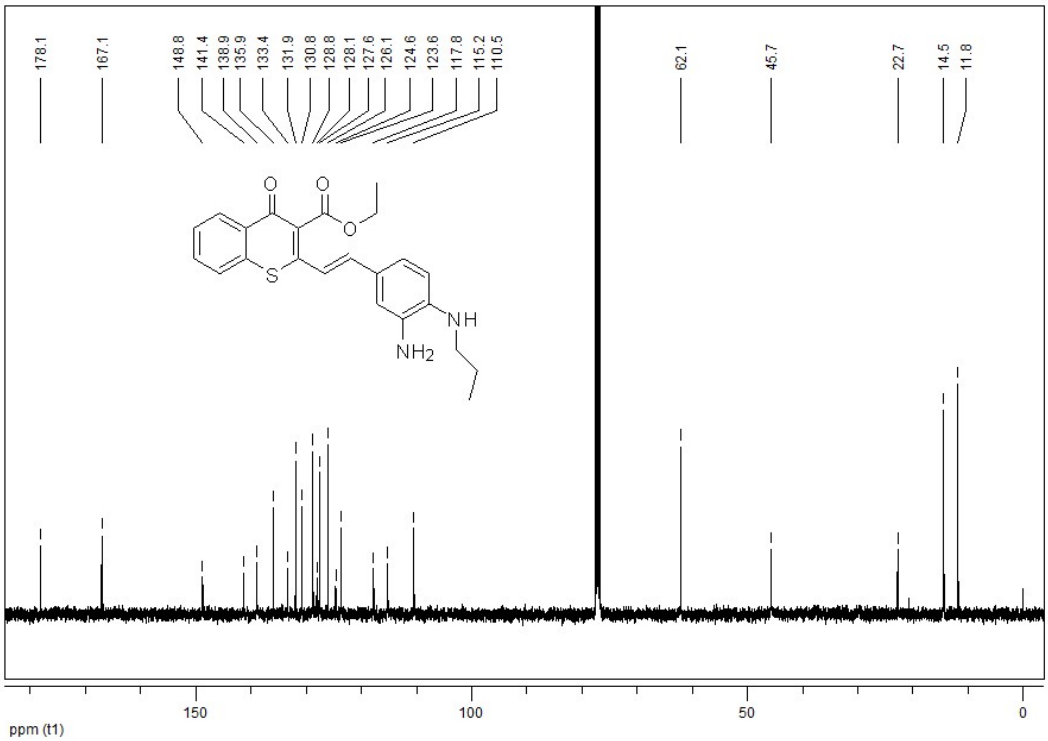

Fig. S46. ^{13}C NMR spectrum of compound **1** (100 MHz, $CDCl_3$)

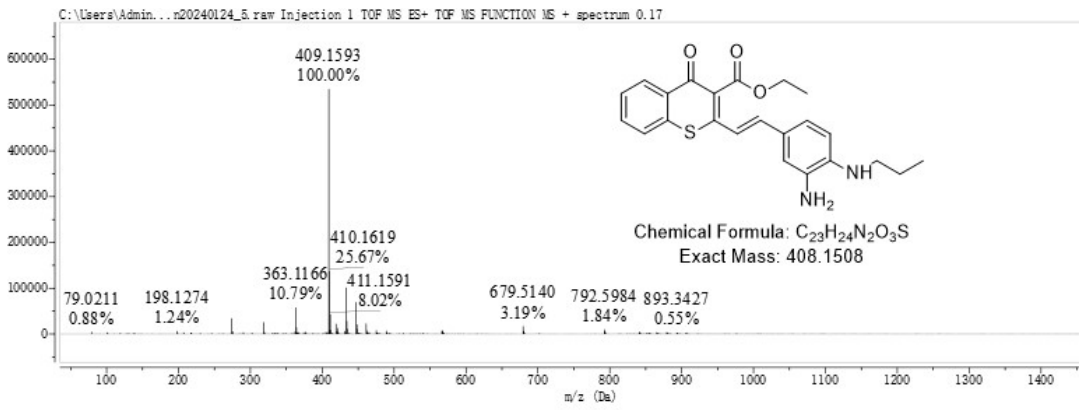

Fig. S47. HRMS (LC/MS) spectrum of **1**. The peak at m/z = 409.1593 was assigned to the mass of [**1** + H^+].

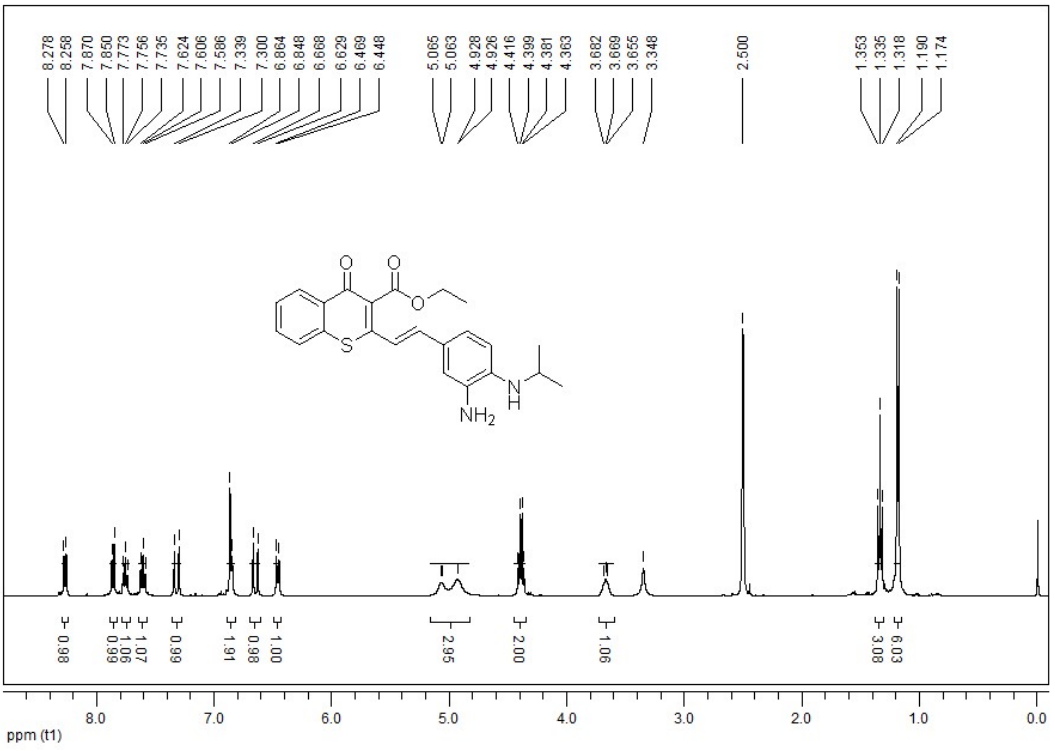

Fig. S48. ^{1}H NMR spectrum of compound **2** (100 MHz, DMSO-d_6)

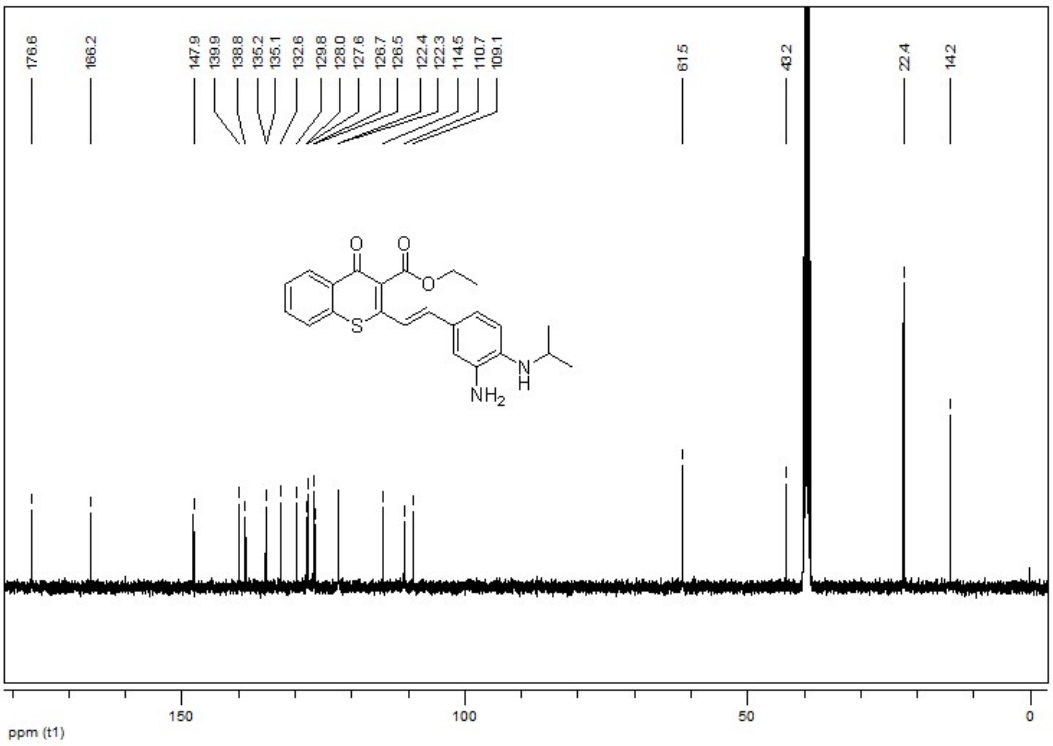

Fig. S49. ^{13}C NMR spectrum of compound **2** (100 MHz, DMSO-d_6)

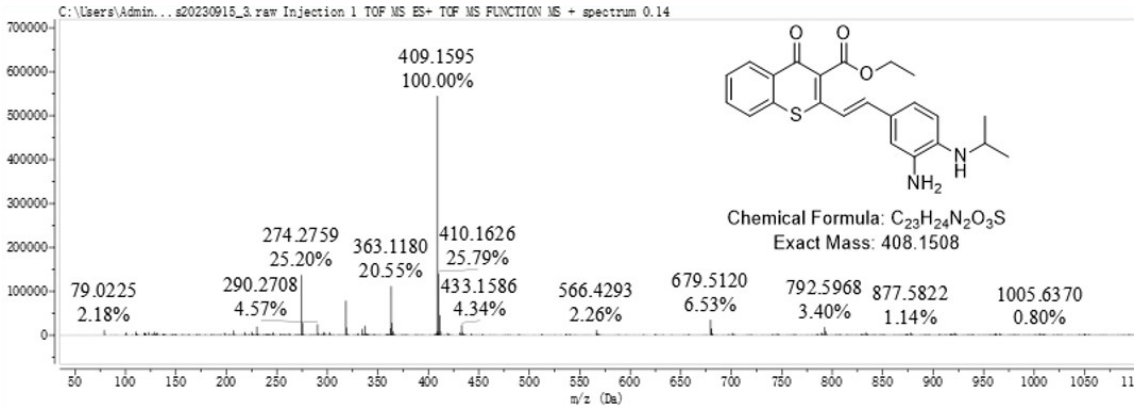

Fig. S50. HRMS (LC/MS) spectrum of **2**. The peak at m/z = 409.1595 was assigned to the mass of [**2** + H^+].

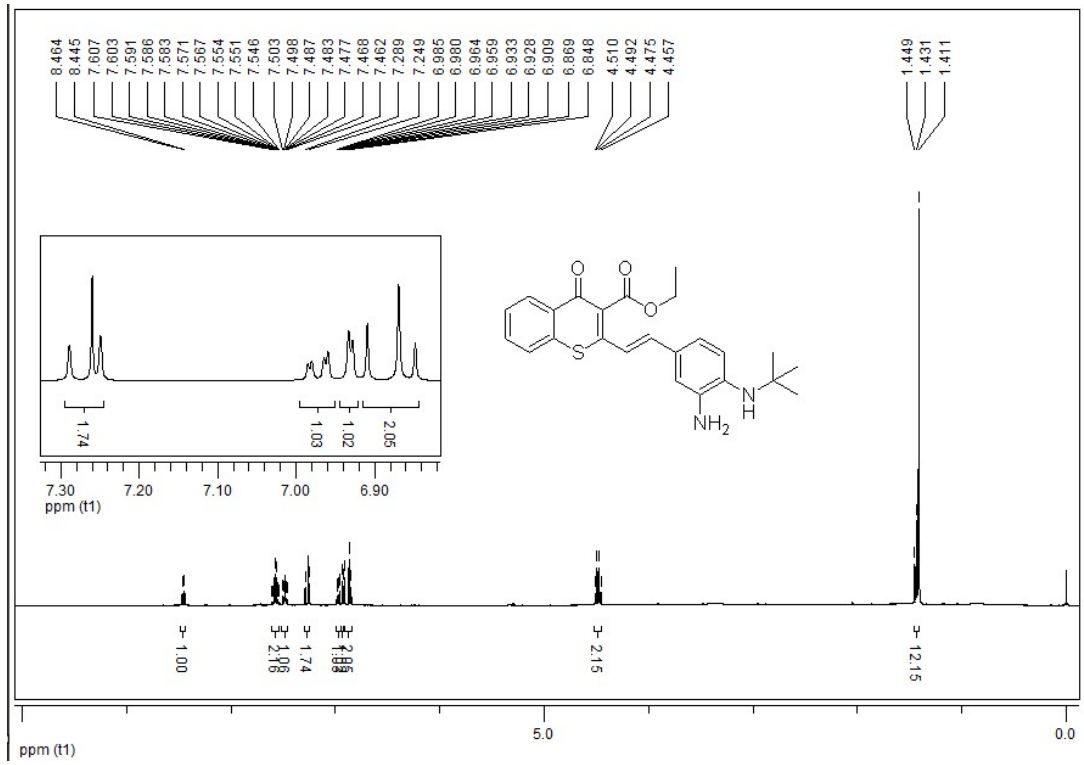

Fig. S51. ^{1}H NMR spectrum of compound **3** (400 MHz, $CDCl_3$)

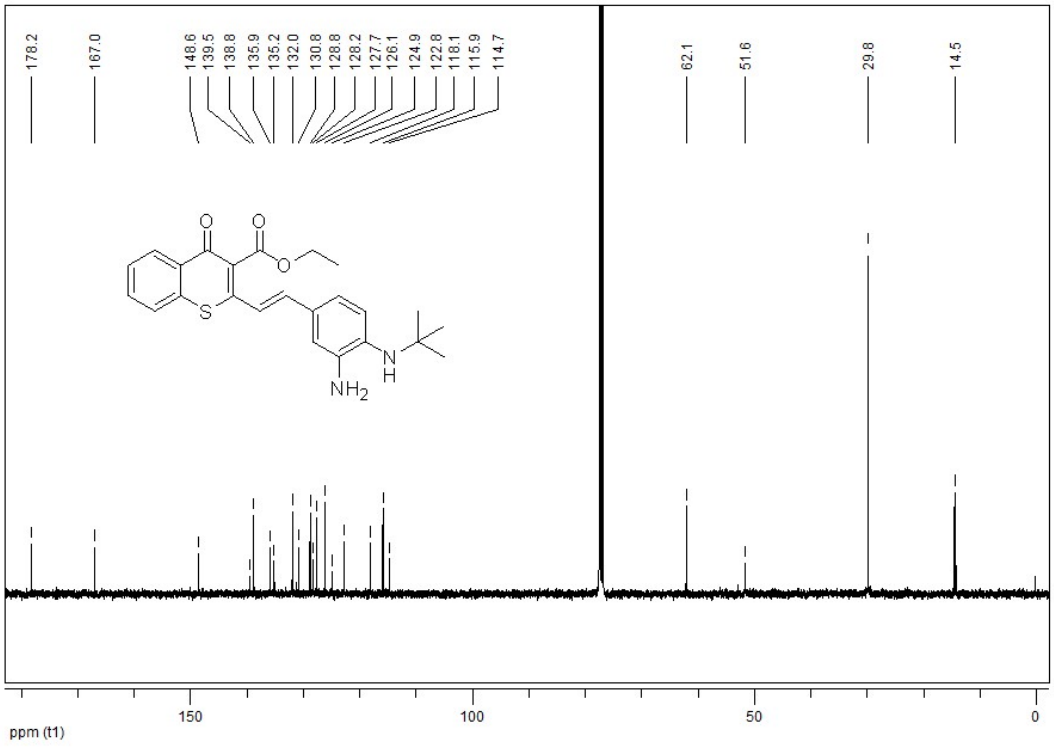

Fig. S52. ^{13}C NMR spectrum of compound **3** (100 MHz, $CDCl_3$)

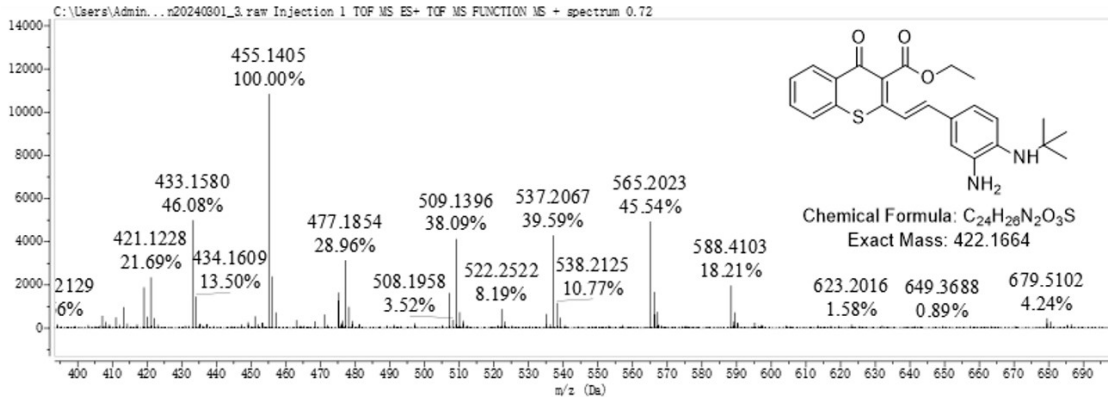

Fig. S53. HRMS (LC/MS) spectrum of **3**. The peak at m/z = 455.1405 was assigned to the mass of [**3** + H^+ + MeOH].

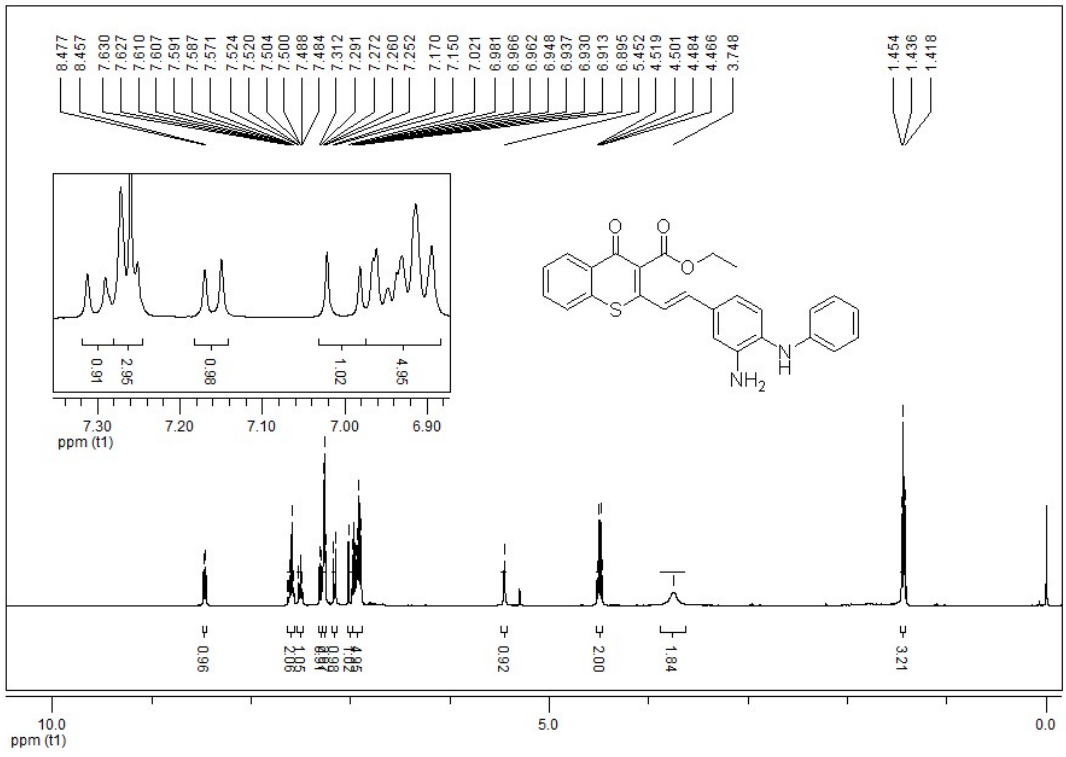

Fig. S54. ^{1}H NMR spectrum of compound **4** (400 MHz, $CDCl_3$)

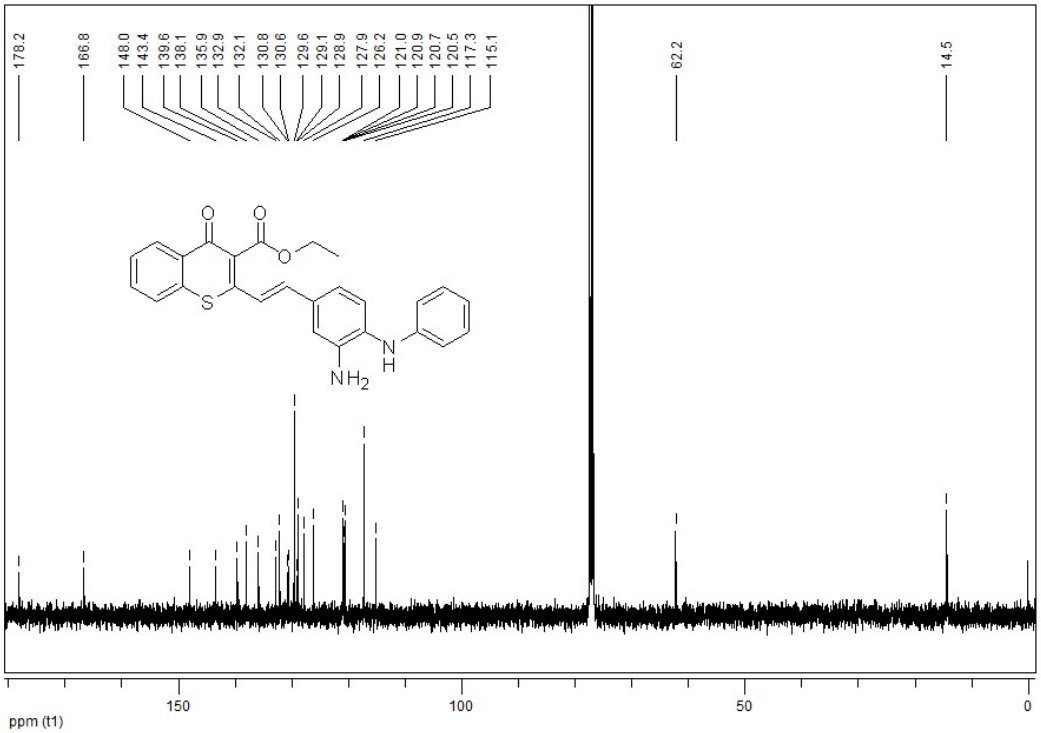

Fig. S55. ^{13}C NMR spectrum of compound **4** (100 MHz, $CDCl_3$)

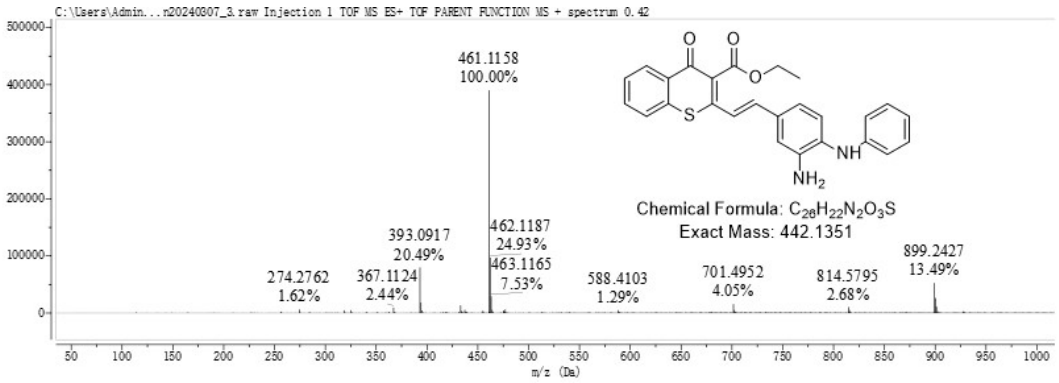

Fig. S56. HRMS (LC/MS) spectrum of **4**. The peak at m/z = 461.1158 was assigned to the mass of [**4** + H^+ + H_2O].

11. The content of glyoxal in real samples

Table S3 The content of glyoxal in real samples

Samples	GO contents	References
Honey	0.1~10.9 mg/kg	[S4]
Makalu honey	3.09~5.13 mg/kg	[S5]
Bread	3.7~12.59 mg/kg	[2a]
Cake	0.01~37 mg/kg	[2a]
Paper	≤1.5 mg/dm^2	[S6]
Cosmetics	≤100 mg/kg	[S7]

12. Reference

[S1] P.K. Wang, J.N. Liu, Y.H. Zhuang, P. Fei, Acylating blueberry anthocyanins with fatty acids: Improvement of their lipid solubility and antioxidant activities, Food Chem.:X 15 (2022) 100420.

[S2] M. Grabolle, M. Spieles, V. Lesnyak, N. Gaponik, A. Eychmüller, U. Resch-Genger, Determination of the fluorescence quantum yield of quantum dots: Suitable procedures and achievable uncertainties, Anal. Chem. 81 (2009) 6285−6294.

[S3] M.Z. Li, C. Liu, W.J. Zhang, L.F. Xu, M.M. Yang, Z.L. Chen, X.X. Wang, L.L. Pu, W.L. Liu, X.S. Zeng, T.H. Wang, An NADH-selective and sensitive fluorescence probe to evaluate living cell hypoxic stress, J. Mater. Chem. B 9 (2021) 9547−9552.

[S4] E. Arena, G. Ballistreri, F. Tomaselli, B. Fallico, Survey of 1,2-dicarbonyl compounds in commercial honey of different floral origin, J. Food Sci. 76 (2011), C1203−C1210.

[S5] S.M. Marshall, K.R. Schneider, K.V. Cisneros, L.W. Gu, Determination of antioxidant capacities, α-dicarbonyls, and phenolic phytochemicals in Florida varietal honeys using HPLC-DAD-ESI-MS^n, J. Agric. Food Chem. 62 (2014), 8623−8631.

[S6] Bundesinstitut für Risikobewertung, XXXVI. Paper and board for food contact. As of 01.07.2015.

[S7] Council directive 76/768/EEC, on the approximation of the laws of the member states relating to cosmetic products, Off. J. Eur. Communities: Legis. 262, 27.9.1976, 169.